Optimal operation of a subsea separation system including a coalescence based gravity separator model and a produced water treatment section

Tamal Das, Sindre Johan Heggheim, Marcin Dudek, Adriaen Verheyleweghen, and Johannes Jäschke*

Department of Chemical Engineering, Norwegian University of Science and Technology Sem Sælandsvei 4, 7491 Trondheim, Norway

E-mail: jaschke@ntnu.no

Abstract

In this work, we develop a model for a gravity separator, and use it together with models from literature to study the control of a subsea separation system that separates oil, gas and water from well fluids in hydrocarbon production. Our separation system contains a gravity separator, hydrocyclones and compact flotation units. The main contributions of the paper are twofold. First, we present a coalescence based dynamic gravity separator model, which is able to predict oil concentration in water outlet and water concentration in oil outlet. Second, we study optimal operation of the overall separation system with an objective of maximizing water removal. We propose a simple control structure that operates the process close to optimally, by rejecting disturbances from upstream flows and maintaining a tight control of the quality of the purified water leaving the system.

Introduction

In the oil and gas industry, separation systems are used to separate hydrocarbons from undesirable components, such as water and sand, which are inevitably produced from wells along with the hydrocarbons. Poorly performing separation systems adversely affect the profitability of the hydrocarbon production system. Crude oil that contains a high water concentration sells at a lower price. Moreover, the transportation of a substandard crude with high water content through an export pipeline may lead to corrosion related damages to the pipeline.[1] Water in the transport line may also give rise to issues with flow assurance in the riser, such as higher hydrostatic pressure drop and emulsion or hydrate formation.
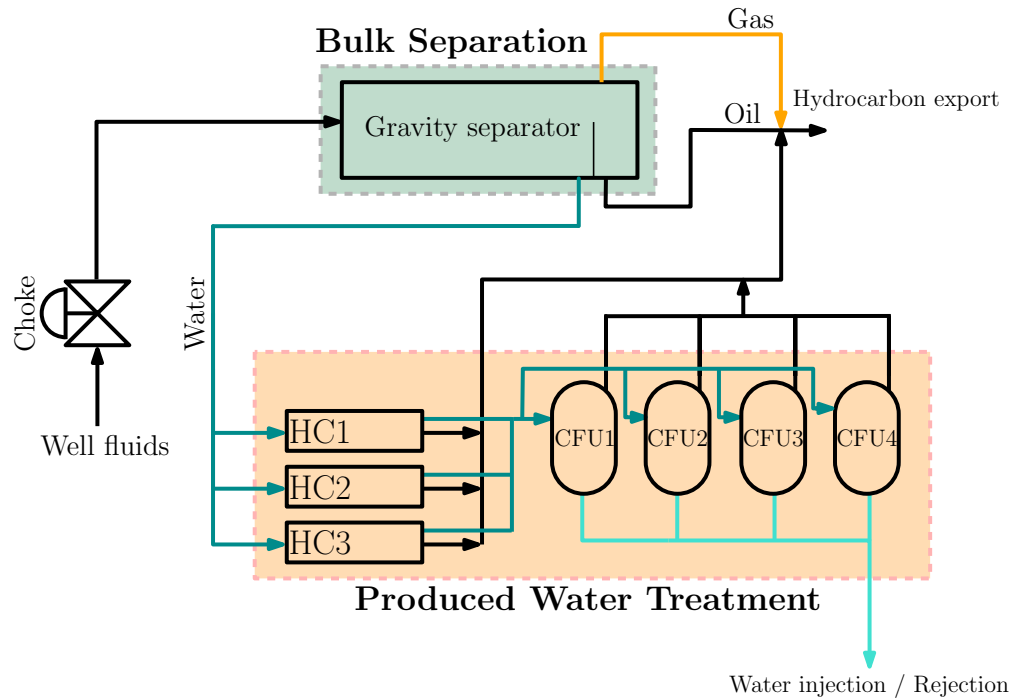

Figure 1: A subsea separation system composed of hydrocyclones (HC) and compact flotation units (CFU). The reject streams from HC and CFU are directed to hydrocarbon export line; slops or other facilities to process the rejects are typically not available subsea. In this figure, we do not show pumps for reject streams and for water injection.

Figure 1 shows a schematic of the separation system we will study further in this paper. This separation system consists of a bulk separation part, consisting of a gravity separator, and a produced water treatment part, consisting of three hydrocyclones (HC) and four

compact flotation units (CFU). A real subsea separation system may follow a similar set-up, albeit with a different number of units, depending on the production rate, fluid properties and compositions.[2] The main operational disturbances to a hydrocarbon separation system are changes in the inlet conditions to the bulk separation, such as pressure, and inflows and compositions of gas, oil and water. Any control structure that aims to operate the system optimally must handle these disturbances well, and consider the system as a whole, in order to account for the interactions between the different components.

Control of upstream separation systems has been considered previously in the literature. For example, Yang et al.[3–5] investigated plant-wide optimal control strategies to a real pilot scale separation system. Their system included a gravity separator and a deoiling hydrocyclone. In their work, they developed a control strategy to operate a combination of the two separators by controlling water level in the gravity separator and the pressure difference ratio (PDR) in the hydrocyclone to their reference values. The main contribution in terms of separation system operation was a unified way of tuning the two controllers so that they work together well.

Ribeiro et al.[6] implemented a model predictive controller (MPC) for set-point control of oil production rate, oil in water (OiW) outlet and water in oil (WiO) outlet from a gravity separator which receives feed from an upstream process of three gas-lifted wells and a riser. The case study is based on well data from Campos Basin field near Rio de Janeiro, Brazil, in which a real time optimization (RTO) layer finds optimal operating points, which are followed and further fine-tuned by the MPC layer. The model used to compute concentrations of oil in water and water in oil is based on polynomial correlations. The gas injection rates for the three wells and the separator water level were used as manipulated variables for the MPC. The results presented show that the controller reacts well to set-point changes and rejects disturbances effectively. The lowest level controllers are PID-controllers, which track the set-points given by the MPC layer.

To avoid the negative consequences of water in the transport system, it has been proposed

to place separation systems close to the production site, and remove the water.[7] This has resulted in several subsea separation facilities, where the separation equipment has been placed on the seabed; among them two facilities - Troll C[8] and Tordis[9,10] are in Norway. Besides water removal on the seabed, subsea separation has many other advantages. Some of them are increased production due to reduced backpressure on the reservoir, need for fewer flowlines/risers, reduced riser based slugging, reduced scaling and corrosion in flowlines and hydrate prevention.[7]

In this paper, we study how to operate such a subsea separation system optimally. The two main contributions in this paper are: A dynamic model for a gravity separator that includes the coalescence of droplets dispersed in the continuous phases in a simplified way, and a simple control structure that operates a separation system close to optimally using simple proportional-integral (PI) controllers. The proposed control solution is easy to implement on the commonly used industrial control systems, and yields good performance in the presence of disturbances while adhering to important process constraints, such as on the water quality.

The problem of maximizing water removal in subsea separation systems has attracted very little attention in literature, especially using first principles models. Besides, in the literature for first-principles based gravity separator models, the phenomenon of droplet-droplet coalescence has either been neglected[11–13] or modeled in a complex way.[14] The droplet-droplet coalescence is an important phenomenon in the context of gravity separation[15] and the literature is lacking a simplified way to address it. In this paper, we fill these two gaps by presenting a control and optimization oriented model that includes coalescence inside the gravity separator, and using it together with other models from literature to study how to operate the overall system optimally.

This paper is organized as follows. The next section presents the gravity separator model that we developed. Thereafter, we present a section on optimal operation of our subsea separation system. Here we discuss a control structure design, and results from optimization

4

and dynamic simulation of the system under disturbances. In the discussion section, we discuss our modeling assumptions and provide guidelines on how to include the effects that have been ignored in our work. In the final section, we conclude the paper with some final remarks.

Coalescence based gravity separator model

Process description

A schematic of a horizontal gravity separation process is shown in Figure 2, in which a horizontal cylindrical vessel is used to perform a bulk separation of well fluids into three phases - oil, gas and water. Gravity separators are quite large in size, such that they provide
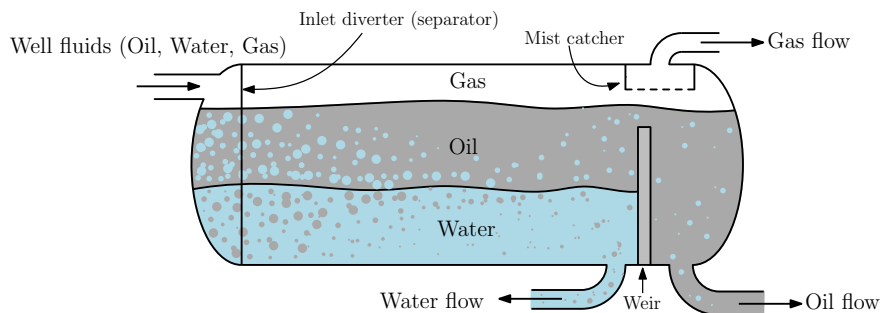
Figure 2: Schematic of a three phase gravity separator

enough residence time for the phases to separate due to gravitational forces. At the inlet of the separator, a multiphase feed usually separates into two liquid layers - a continuous water layer at the bottom and a continuous oil layer above the water layer, and a gas phase on top. Within each layer, the difference in densities of the different phases causes the droplets of dispersed phase to sediment or rise. The oil dispersed in the continuous water phase rises and the water dispersed in continuous oil phase sediments. At the end of the separator, a weir plate separates the oil flow from the water flow. The water is removed from an outlet before the weir and the oil is removed from an outlet after the weir. The gas phase is removed from an outlet at the top, typically after a mist catcher.

Gravity separators are designed to facilitate the separation of the dispersed phase i.e. oil in water and water in oil from the respective continuous medium. Therefore, inside the separator, breakage of the dispersed droplets is sought to be minimized, while droplet-droplet coalescence, which makes droplets grow larger in size, is enhanced[15] because larger droplets rise or sediment faster than smaller ones. Once the droplets reach the oil-water interface, they merge with their respective continuous medium. The nature of coalescence, either droplet-droplet or droplet-interface, is determined by the contact time between the coalescing entities and the rate of drainage of the thin film of the continuous phase in between the coalescing entities.[16,17]

Previous work in control-oriented gravity separator modeling

For the purpose of control, models that involve complex computational fluid dynamics (CFD) calculations[18][19] are generally not useful because they are computationally too expensive. Likewise, models that describe the gravity separation phenomenon in a batch process[20–23] are not directly transferable to industrial-size separation system, such as the one studied in this paper.

There are a handful of works in control-oriented continuous gravity separator modeling. A simplified three phase separator model was developed by Sayda and Taylor,[11] in which they consider two lumped bulk liquid phases. Oil droplets of diameter 500 μm are considered to be dispersed in the water phase at the start of the separator; these droplets separate from the water phase and move to the oil phase based on Stokes' law. The droplets that fail to move to the oil phase continue further into the water outflow. No dispersed water in the oil phase is considered. Vapor-liquid equilibrium is assumed at the oil surface using Raoult's law. Hence, the model can predict oil and gas fractions in the oil phase and oil, gas and water fractions in the water phase in a dynamic way.

Backi and Skogestad[13] developed a dynamic gravity separator model considering a static distribution of droplet classes, ranging in size from 50 μm to 500 μm. These droplet classes

are considered for the oil droplets dispersed in the water phase as well as the water droplets dispersed in the oil phase. All water droplets are considered to be located at the top edge of the oil phase whereas all oil droplets at the bottom edge of the water phase at the start of the separator. The oil and water phases are horizontally distributed into five control volumes. In order to calculate the droplet distribution out of each control volume, a comparison is made between horizontal residence time and vertical residence time of a droplet within the control volume, where the vertical residence time is calculated using Stokes' law. The vertical position of a droplet out of a control volume determines if the droplet merges with its continuous phase or proceeds further horizontally. No coalescence or breakage of the droplets is considered. The results show dynamic changes in the droplet distribution in the two continuous phases at the separator outlet under changes in water level set-point. This model was extended by Backi et al.[14] by considering population balance equations to determine the precise droplet distribution entering the separator. The population balances, which consider both the coalescence and the breakage phenomena, are implemented on only a small control volume just before the first of the five main control volumes, thereby ignoring the coalescence or the breakage phenomena in those five control volumes.

Das et al.[12] developed a simplified gravity separator model based on a three layer approximation, where an additional layer called dense-packed layer or emulsion layer is added in between the water and the oil layers.[24] The models discussed above do not consider this third layer. This layer can occur in some cases due to surface properties imparted by some of the chemicals, such as asphaltenes present in certain crude oils, which hinder the separation process.[25–27] This model considers three lumped layers with no spacial distribution and can describe the oil fraction in all these layers dynamically.

None of the models described above considers the effect of coalescence of droplets inside the gravity separator. In this paper, we fill the gap of a simplified dynamic model for gravity separator that includes the important phenomenon of dispersed phase coalescence inside the gravity separator in a simplified way.
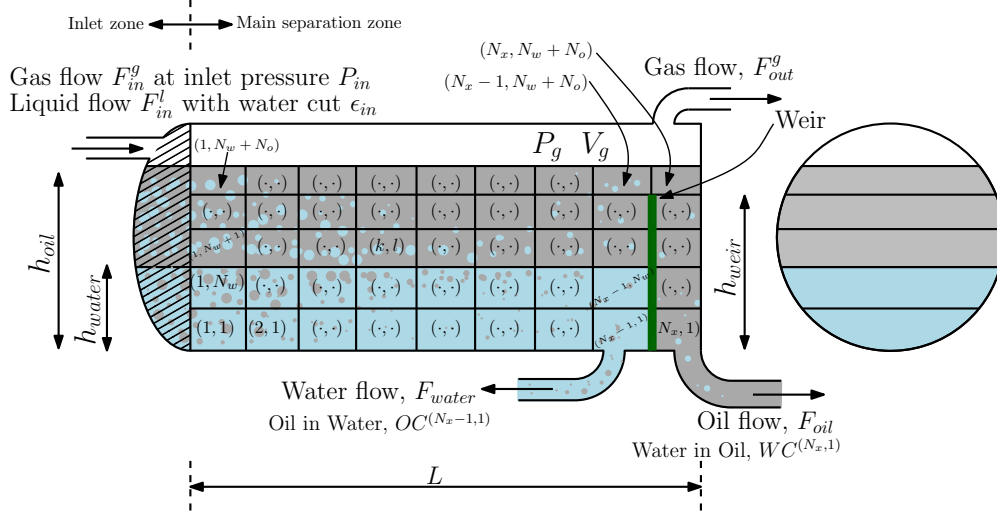
Model description

Figure 3: Three phase gravity separator divided into control volumes $V^{k,l}$. The control volumes are indexed by (k, l), where k spans from $k = 1$ to N_x traveling from left to right, while l spans from $l = 1$ to $(N_w + N_o)$, traveling from bottom to top. In this figure, we have $N_x = 9, N_w = 2$ and $N_o = 3$.

Figure 3 shows a schematic of our proposed model and its different elements. The model considers two zones - an inlet zone and a main separation zone. In the inlet zone, an initial separation of the fluids into two bulk layers happens, whereas in the main separation zone the sedimentation of the water droplets in the continuous oil layer and the creaming of the oil droplets in the continuous water layer happens. When the dispersed droplets reach the interface, they merge with their respective continuous phase by crossing the oil-water interface. At the end of the main separation zone, the water layer with the remaining oil dispersed in it adjacent to the weir exits the water outlet of the separator. The oil with remaining dispersed water above the interface and just left of weir goes over the weir and is collected from the oil outlet.

Inlet zone

It is assumed that an initial instantaneous separation of the fully mixed multiphase flow happens in the inlet zone of the separator, shown by the area in rising tiling pattern in

8

Figure 3. Due to the initial separation, a fraction γ_w of net water inflow to the separator enters the continuous water layer. Likewise, a fraction γ_o of net oil inflow to the separator enters the continuous oil layer, as is also assumed by Backi and Skogestad.[13] The rest of the oil remains dispersed in the water layer and enters the main separation zone. Similarly, the water that does not form the continuous water phase remains dispersed in the continuous oil layer and enters the main separation zone.

Control volumes

To derive the model, the main separation zone is divided into several control volumes indexed by (k, l) as shown in Figure 3. The discretization we use ensures that the oil-water interface is not inside a control volume. The water layer, i.e. the volume of liquid below the oil-water interface is divided into $(N_x - 1)$ equally spaced horizontal sections and N_w equally spaced vertical sections, leading to $N_w(N_x - 1)$ control volumes. A part of the oil layer (the liquid volume above the oil-water interface) that is below the weir height, and left of the weir is divided into $(N_x - 1)$ equally spaced horizontal sections and $(N_o - 1)$ equally spaced vertical sections, leading to $(N_o - 1)(N_x - 1)$ more control volumes. There is one vertical section and $(N_x - 1)$ equally spaced horizontal sections for the part of the oil layer above the weir height and to the left of the weir plate, which lead to $(N_x - 1)$ more control volumes. On the right side of weir, there is one horizontal section and $(N_w + N_o)$ vertical sections. Therefore, we consider a total of $N_x(N_w + N_o)$ control volumes in our model. The volume of control volume (k, l) is denoted by $V^{(k,l)}$.

Figure 3 also introduces some important notation: F_{in}^g denotes inlet gas flow, P_{in} inlet pressure, F_{in}^l inlet liquid flow, ϵ_{in} inlet water cut in the liquid flow, F_{out}^g gas outflow, F_{oil} oil outflow right of weir, h_{oil} total liquid level, h_{water} water level, $WC^{(N_x,1)}$ water cut in oil outflow, F_{water} water outflow left of weir, $OC^{(N_x-1,1)}$ oil cut in the water outflow, P_g separator pressure as well as the outlet gas pressure, V_g the volume available for gas phase above the liquid volume, h_{oil} oil level or total liquid level and h_{water} water level. The separator volume

9

is assumed to be a perfect cylinder, and all water and oil cuts and fractions are volumetric, if not stated otherwise.

Flows through control volume boundaries

We assume that the flows above and below the oil-water interface can be described as independent plug flows, largely given by the outflows F_{oil} and F_{water}, respectively. To obtain the horizontal flow out of the right edge of a control volume, the total flow out of the layer in which the control volume exists is scaled by the cross-sectional area of the control volume normal to the direction of horizontal flow. The horizontal flow out of the right edge of a control volume is then back propagated to find the inflow from the left edge of the same control volume such that the total inflow to the control volume equals the total outflow from the control volume. A special scenario occurs when the oil outflow F_{oil} is lower than the downward flow through interface, this will lead to a flow in backward direction (or an outflow from the left side), also known in this work as back flow.

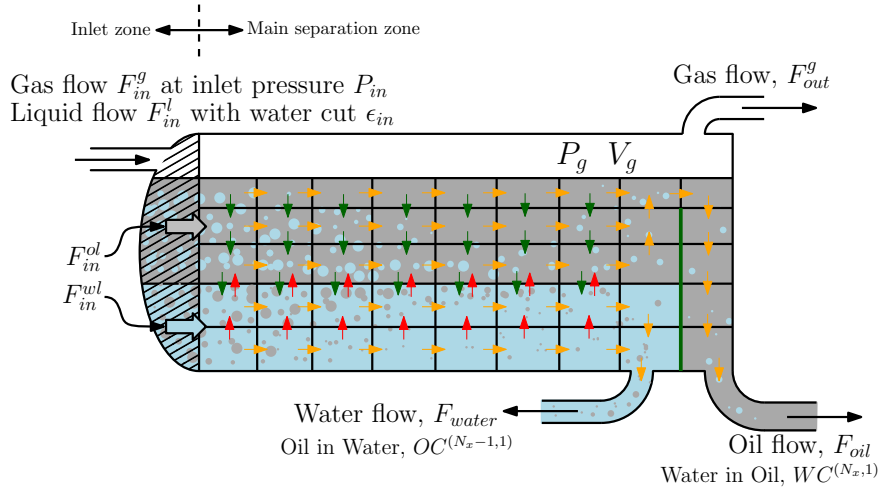The modeled flows are illustrated in Figure 4. We denote convective flows as the mass

Figure 4: Flows for each control volume in the gravity separator model. Convective flows (due to bulk motion) are colored in orange. Non-convective (buoyancy-driven) water flows are colored in green. Non-convective (buoyancy-driven) oil flows are colored in red.

transport due to the bulk movement, while the flows driven by buoyancy are referenced to as

non-convective flows. For the control volumes $(1, 1 \ldots (N_w + N_o))$, i.e the ones on the most left and adjacent to the inlet zone, the inflows from the left edge are decided by the liquid inflows to the separator. The flow entering the oil layer F_{in}^{ol} and the water layer F_{in}^{wl} are

$$F_{in}^{ol} = \gamma_o(1 - \epsilon_{in})F_{in}^l + (1 - \gamma_w)\epsilon_{in}F_{in}^l, \tag{1}$$

and

$$F_{in}^{wl} = \gamma_w\epsilon_{in}F_{in}^l + (1 - \gamma_o)(1 - \epsilon_{in})F_{in}^l. \tag{2}$$

These flows are scaled by the cross-sectional area of the control volumes normal to the direction of horizontal flow to obtain the inflows on the left edges of each of the control volumes $(1, 1 \ldots (N_w + N_o))$. The convective flows out of the right edge of the control volumes just left of the weir are considered zero. The convective flows out of these control volumes are directed downwards if the fluid is below the oil-water interface and upwards otherwise.

The settling velocity of droplets in gravity separators is described by the Stokes' law, which gives the terminal velocity of the dispersed phase relative to the continuous phase in or away from the direction of gravity based on whether the dispersed phase is heavier or lighter than the continuous phase, respectively. The terminal velocity v_s from Stokes' law is

$$v_s = \frac{\triangle \rho g d^2}{18\mu}, \tag{3}$$

where g denotes the acceleration due to gravity, d the diameter of the dispersed phase droplet, $\triangle \rho$ the difference between the densities of the dispersed phase and the continuous phase and μ the viscosity of the continuous phase. From this expression, it is clear that a higher $\triangle \rho$, a larger d and a smaller μ are favorable for a fast separation. In particular, the diameter of the droplets significantly affects the velocity due to the quadratic term in Eq. 3, which makes the droplet-droplet coalescence an important phenomenon in a gravity separator. The terminal velocity given by Stokes' law Eq. 3 is valid for one single droplet in an infinite continuum, which is not the case in this model. There are often other dispersed phase droplets in the

vicinity. Especially for a control volume in the oil layer at the interface, the flow of the water droplets crossing the top edge of the control volume downwards is given by the area of downward transfer multiplied by terminal velocity of dispersed water. If we consider a control volume in the oil layer near the oil-water interface, e.g. $(k, N_w + 1)$ and the mass transfer of water through the interface is low or hindered and we use Eq. 3 to compute non-convective flow of water downwards at the top edge, it is possible that the water content in this control volume surpasses 1, which is unphysical (shown in Figure 5).
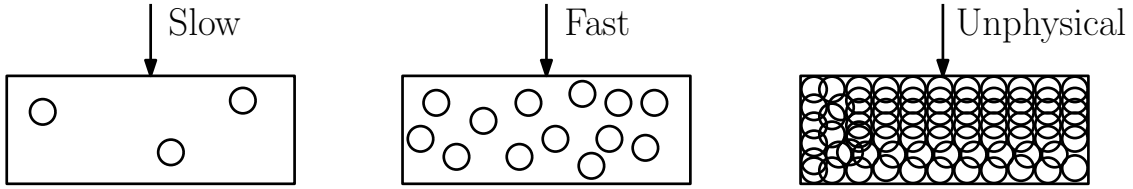

Figure 5: Scenarios faced by sedimenting water droplets while entering a control volume

A similar situation can occur in the control volumes just below the oil-water interface, in which the oil content in those control volumes surpasses 1. To avoid these unphysical scenarios, we adapted the Stokes' equation as

$$
v_a = \begin{cases} v^s \left(\frac{WC_p - WC_{receiver}}{WC_p} \right) & \text{for Water in Oil} \\ v^s \left(\frac{OC_p - OC_{receiver}}{OC_p} \right) & \text{for Oil in Water} \end{cases}, \tag{4}
$$

where v_a denotes the adapted terminal velocity, and $WC_{receiver}$ and $OC_{receiver}$ water cut in a control volume in the oil layer and oil cut in a control volume in the water layer, respectively. WC_p denotes phase inversion point in terms of water cut and OC_p in terms of oil cut. The adapted terminal velocity v_a for droplets moving out of a control volume (k, l) is denoted by $v_a^{(k,l)}$. The key consideration in this adaptation is that a higher dispersed phase content in a control volume results in a lower non-convective flow entering that control volume. Thereby, a higher water cut in a control volume in the oil layer will have a lower non-convective flow of dispersed water droplets entering that control volume.

Number densities of droplet classes

There are N_d droplet classes considered in the model. The droplet classes are identified by subscript i. These classes are chosen such that the droplet volume of these classes are integer multiples of the droplet volume of the smallest base class $i = 1$, which has a droplet diameter d_A and volume $V_A = \left(\frac{\pi d_A^3}{6}\right)$. This choice is governed by the idea that droplets coalesce with other droplets to become larger droplets that will have volumes in multiples of the volume of a droplet in the base class $i = 1$. The droplet class i indicates that the volume of a droplet in that class is iV_A and thereby, the diameter of droplets in that droplet class is $d_A \sqrt[3]{i}$. The dispersed phases entering control volumes $(1, l)$ are assumed to consist of droplets of the smallest size d_A i.e. only of droplet class $i = 1$ for both oil dispersed in water and water dispersed in oil.

To keep notation light, we use the subscript i to denote the droplet classes in both continuous phases, that is in the oil layer, the subscript i denotes droplet class for droplets of water, whereas in the water layer, it denotes the droplet class for droplets of oil. The total number of droplets of class i in control volume (k, l) is given by $N_i^{(k,l)}$. The corresponding number density of that droplet class in the control volume is calculated by dividing the densities of the droplets by the volume of the control volume as $n_i^{(k,l)} = \frac{N_i^{(k,l)}}{V^{(k,l)}}$. The partial density is defined as

$$\rho_i^{(k,l)} = \rho_d n_i^{(k,l)} (iV_A),\tag{5}$$

where ρ_d is the density of the dispersed phase, which is either pure water phase density ρ_w or pure oil phase density ρ_o. The total partial density of a dispersed phase in a control volume can be given as a summation of the partial densities for the N_d droplet classes by

$$\rho_d^{(k,l)} = \sum_{i=1}^{i=N_d} \rho_i^{(k,l)},\tag{6}$$

where the subscript d denotes the dispersed phase, either water in the continuous oil layer or oil in the continuous water layer. The vector of stacked number densities for different

droplet size classes starting from the smallest to the largest class is denoted by $\bar{n}^{(k,l)}$ and the same for partial densities by $\bar{\rho}^{(k,l)}$. The volume fraction of the dispersed phase in a control volume is

$$\epsilon_d^{(k,l)} = \frac{\rho_d^{(k,l)}}{\rho_d}. \tag{7}$$

Hence, water cut in any control volume in the oil layer is given by

$$WC^{(k,l)} = \frac{\rho_w^{(k,l)}}{\rho_w}, \tag{8}$$

and oil cut in any control volume in the water layer is given by

$$OC^{(k,l)} = \frac{\rho_o^{(k,l)}}{\rho_o}. \tag{9}$$

Droplet-droplet coalescence

The droplet-droplet coalescence is modeled using a set of $N_{reaction}$ reactions in order to result in N_d droplet size classes. The reactions are shown below with each reaction being identified by a subscript j. The reactions can be expressed in a general form in volume terms with species expressed as multiples of V_A as

$$\alpha V_A + \beta V_A \xrightarrow{k_d} (\alpha + \beta) V_A, \tag{10}$$

where,

$$\{\alpha, \beta : \alpha, \beta \in [1, \ldots, (N_d - 1)], (\alpha + \beta) \leq N_d\} \tag{11}$$

The reaction rate r_j for reaction j is given by

$$r_j = k_d n_\alpha^{(k,l)} n_\beta^{(k,l)}, \tag{12}$$

where the unit of reaction rates is $\left[\frac{1}{m^3 s}\right]$, α and β both are one of the droplet classes. For

14

simplicity, we assume that the droplet-droplet coalescence reaction rate constants k_d are same for all the reactions, irrespective of whether the dispersed phase is oil in water or water in oil, but this assumption can be relaxed if necessary. The parameter k_d has a unit of $\left[\frac{m^3}{s}\right]$. The rates for these $N_{reaction}$ reactions stacked in a $N_{reaction} \times 1$ vector of reaction rates is denoted by $\bar{r}$. The stoichiometry for the reactions of the N_d droplet classes is stored in a $N_d \times N_{reaction}$ stoichiometric matrix S using Eq. 10.

Droplet-Interface coalescence

The water droplets in the oil layer just above the oil-water interface can merge with the continuous water layer, whereas the oil droplets in the water layer just below the oil-water interface can merge with the continuous oil layer. We assume that there is no backmixing through the interface, i.e. once a water droplet has entered the continuous water phase, it remains there. Similarly, once an oil droplet enters the continuous oil phase, it stays there. Assuming incompressible liquids, we calculate the mass transfer (in volumetric terms) through the interface as

$$q_{w,int,\downarrow}^{(k,l)} = k_w^{int} A_{int}^{(k,l)} W C^{(k,l)}, \tag{13}$$

and

$$q_{o,int,\uparrow}^{(k,l)} = k_o^{int} A_{int}^{(k,l)} O C^{(k,l)}, \tag{14}$$

where, $q_{w,int,\downarrow}^{(k,l)}$ denotes water flow from control volume (k,l) across the interface downwards into the continuous water layer. Similarly, $q_{o,int,\uparrow}^{(k,l)}$ denotes oil flow from control volume (k,l) across the interface upwards into the continuous oil layer. The terms k_w^{int} and k_o^{int} denote mass transfer coefficients with units $[m/s]$, and $A_{int}^{(k,l)}$ the interfacial area that is part of the oil-water interface associated with the control volume (k,l). The net transfer of mass through the interface is $\left(q_{w,int,\downarrow}^{(k,l)} - q_{o,int,\uparrow}^{(k,l)}\right)$ in the downward direction or $\left(q_{o,int,\uparrow}^{(k,l)} - q_{w,int,\downarrow}^{(k,l)}\right)$ in the upward direction.

Mass balances for dispersed phases

A mass balance for mass of droplets of a droplet class i in a control volume (k, l) is

$$\frac{dm_i^{(k,l)}}{dt} = \dot{m}_{i,in}^{(k,l)} - \dot{m}_{i,out}^{(k,l)} + \dot{m}_{i,gen}^{(k,l)} - \dot{m}_{i,cons}^{(k,l)}, \tag{15}$$

where, $\dot{m}_{i,in}^{(k,l)}$ denotes the inflow of mass of droplets in class i into control volume (k, l), $\dot{m}_{i,out}^{(k,l)}$ outflow of mass of droplets in class i from control volume (k, l), $\dot{m}_{i,gen}^{(k,l)}$ rate of gain of mass due to generation of droplets in class i in control volume (k, l) and $\dot{m}_{i,cons}^{(k,l)}$ rate of loss of mass due to consumption of droplets in class i in control volume (k, l). The generation and the consumption terms are due to coalescence, whereas inflow and outflow terms appear due to convective flow in the horizontal or vertical direction and non-convective flow in the vertical direction due to Stokes' law. Combining Eq. 15 for all the droplet classes in a vector, we obtain the mass balance of the dispersed phase in control volume (k, l) as

$$\frac{d\bar{m}^{(k,l)}}{dt} = \dot{\bar{m}}_{in}^{(k,l)} - \dot{\bar{m}}_{out}^{(k,l)} + \dot{\bar{m}}_{gen}^{(k,l)} - \dot{\bar{m}}_{cons}^{(k,l)}, \tag{16}$$

Partial densities of dispersed phase droplet classes

The left hand side of Eq. 16 can be rewritten as

$$\frac{d\bar{m}^{(k,l)}}{dt} = V^{(k,l)} \frac{d\bar{\rho}^{(k,l)}}{dt} + \bar{\rho}^{(k,l)} \frac{dV^{(k,l)}}{dt}, \tag{17}$$

which is used to rewrite Eq. 16 as

$$\frac{d\bar{\rho}^{(k,l)}}{dt} = \frac{1}{V^{(k,l)}} \left(\dot{\bar{m}}_{in}^{(k,l)} - \dot{\bar{m}}_{out}^{(k,l)} + \dot{\bar{m}}_{gen}^{(k,l)} - \dot{\bar{m}}_{cons}^{(k,l)} - \bar{\rho}^{(k,l)} \frac{dV^{(k,l)}}{dt} \right). \tag{18}$$

As inflow $\dot{\bar{m}}_{in}^{(k,l)}$ and outflow $\dot{\bar{m}}_{out}^{(k,l)}$ are both made up of convective and non-convective flows, we can expand the expressions for the net flows as

$$\dot{m}_{in}^{(k,l)} - \dot{m}_{out}^{(k,l)} = \left(\dot{m}_{in,conv}^{(k,l)} + \dot{m}_{in,non-conv}^{(k,l)} \right) - \left(\dot{m}_{out,conv}^{(k,l)} + \dot{m}_{out,non-conv}^{(k,l)} \right) \qquad (19)$$

$$= \left(\dot{m}_{in,conv}^{(k,l)} - \dot{m}_{out,conv}^{(k,l)} \right) + \left(\dot{m}_{in,non-conv}^{(k,l)} - \dot{m}_{out,non-conv}^{(k,l)} \right) \qquad (20)$$

$$= \triangle \dot{m}_{conv}^{(k,l)} + \triangle \dot{m}_{non-conv}^{(k,l)} \qquad (21)$$

Similarly, the terms $\dot{m}_{gen}^{(k,l)}$ and $\dot{m}_{cons}^{(k,l)}$ can be related to the coalescence reaction rates as

$$\left(\dot{m}_{gen}^{(k,l)} - \dot{m}_{cons}^{(k,l)} \right) = (\rho_d V_A) \, \mathbb{1} \circ \left(S\bar{r}V^{(k,l)} \right) = R^{(k,l)}, \qquad (22)$$

where $R^{(k,l)}$ is the rate of gain of mass due to coalescence reactions in control volume (k,l) for all droplet classes stacked in a vector, and $\mathbb{1} = [1, 2, \ldots, N_d]^T$. Here, the operator $\circ$ denotes element wise multiplication of matrices.

Using Eq. 21 and Eq. 22 in Eq. 18, we obtain

$$\frac{d\bar{\rho}^{(k,l)}}{dt} = \frac{1}{V^{(k,l)}} \left(\triangle \dot{m}_{conv}^{(k,l)} + \triangle \dot{m}_{non-conv}^{(k,l)} + R^{(k,l)} - \bar{\rho}^{(k,l)} \frac{dV^{(k,l)}}{dt} \right). \qquad (23)$$

The derivative $\frac{dV^{(k,l)}}{dt}$ is a function of $\frac{dh_{water}}{dt}$ and $\frac{dh_{oil}}{dt}$, which can be found in the thesis work of Heggheim.[28]

The equations for the control volumes depend on their positioning given by the seven regions in Figure 6.

For control volumes $(1 \ldots (N_x - 2), 1 \ldots (N_w - 1))$ (Region I in Figure 6): These are the control volumes in the water layer not adjacent to the oil-water interface, excluding the ones adjacent to the weir. Under normal conditions when no back flow is happening

$$\triangle \dot{m}_{conv}^{(k,l)} = \bar{\rho}^{(k-1,l)} q_{x,left}^{(k,l)} - \bar{\rho}^{(k,l)} q_{x,right}^{(k,l)} \qquad (24)$$

will hold, where $q_{x,left}^{(k,l)}$ and $q_{x,right}^{(k,l)}$ denote the rightward flows on the left and the right edges,
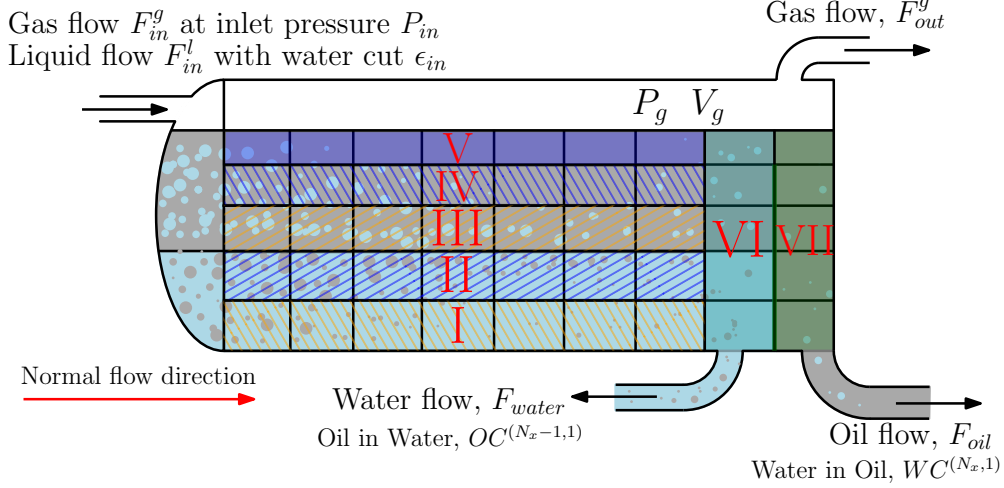
Figure 6: Control volume regions with different set of equations

respectively of the control volume (k, l). The term $q_{x,left}^{(k,l)}$ for control volume $(1, 1)$ is F_{in}^{wl} scaled to the area corresponding to the control volume. The term $\bar{\rho}^{(k-1,l)}$ for control volume $(1, 1)$ is the partial density vector in the feed. The feed flow to the water layer has an oil volume fraction of

$$\epsilon_{in}^{wl} = \frac{(1 - \gamma_o)(1 - \epsilon_{in})F_{in}^l}{(1 - \gamma_o)(1 - \epsilon_{in})F_{in}^l + \gamma_w \epsilon_{in} F_{in}^l}. \tag{25}$$

During transient operation and due to disturbances, the flow directions may change, and this is taken into account by

$$\triangle \dot{m}_{conv}^{(k,l)} = \max\left(\bar{\rho}^{(k-1,l)} q_{x,left}^{(k,l)}, -\bar{\rho}^{(k+1,l)} q_{x,right}^{(k,l)}\right) - \max\left(\bar{\rho}^{(k,l)} q_{x,right}^{(k,l)}, -\bar{\rho}^{(k,l)} q_{x,left}^{(k,l)}\right). \tag{26}$$

For the bottom-most control volumes, the term

$$\triangle \dot{m}_{non-conv}^{(k,l)} = -\bar{\rho}^{(k,l)} v_a^{(k,l)} A_{top}^{(k,l)}, \tag{27}$$

where $A_{top}^{(k,l)}$ denotes the area of the top surface of the control volume (k, l). This surface is the surface through which the droplets of oil travel upwards. There is no positive contribution in $\triangle \dot{m}_{non-conv}^{(k,l)}$ because the bottom surfaces of the control volumes are the separator bottom.

18

For the control volumes that are not at the separator bottom, the term

$$\triangle \dot{m}_{non-conv}^{(k,l)} = \bar{\rho}^{(k,l-1)} v_a^{(k,l-1)} A_{top}^{(k,l-1)} - \bar{\rho}^{(k,l)} v_a^{(k,l)} A_{top}^{(k,l)}. \tag{28}$$

For control volumes $(1 \ldots (N_x - 2), N_w)$ (Region II in Figure 6): $\triangle \dot{m}_{conv}^{(k,l)}$ is identical to that in Eq. 26, while the term

$$\triangle \dot{m}_{non-conv}^{(k,l)} = \bar{\rho}^{(k,l-1)} v_a^{(k,l-1)} A_{top}^{(k,l-1)} - \rho_o q_{o,int,\uparrow}^{(k,l)}. \tag{29}$$

For control volumes $(1 \ldots (N_x - 2), (N_w + 1))$ (Region III in Figure 6): The term

$$\triangle \dot{m}_{conv}^{(k,l)} = \bar{\rho}^{(k-1,l)} q_{x,left}^{(k,l)} - \bar{\rho}^{(k,l)} q_{x,right}^{(k,l)}, \tag{30}$$

where $q_{x,left}^{(k,l)}$ for control volume $(1, N_w + 1)$ is F_{in}^{ol} scaled to the area corresponding to the control volume. An adaptation similar to that in Eq. 26 is also valid for Eq. 30 to account for backflow in the oil layer. The term $\bar{\rho}^{(k-1,l)}$ for control volume $(1, N_w + 1)$ is the partial density vector in the feed. The feed flow to the oil layer has a water volume fraction of

$$\epsilon_{in}^{ol} = \frac{(1 - \gamma_w)\epsilon_{in} F_{in}^l}{\gamma_o(1 - \epsilon_{in}) F_{in}^l + (1 - \gamma_w)\epsilon_{in} F_{in}^l}. \tag{31}$$

The term
$$\triangle \dot{m}_{non-conv}^{(k,l)} = \bar{\rho}^{(k,l+1)} v_a^{(k,l+1)} A_{top}^{(k,l)} - \rho_w q_{w,int,\downarrow}^{(k,l)}. \tag{32}$$

For control volumes $(1 \ldots (N_x - 2), (N_w + 2) \ldots (N_w + N_o - 1))$ (Region IV in Figure 6): The term $\triangle \dot{m}_{conv}^{(k,l)}$ is identical to that in Eq. 30. The term

$$\triangle \dot{m}_{non-conv}^{(k,l)} = \bar{\rho}^{(k,l+1)} v_a^{(k,l+1)} A_{top}^{(k,l)} - \bar{\rho}^{(k,l)} v_a^{(k,l)} A_{top}^{(k,l-1)}. \tag{33}$$

For control volumes $(1 \ldots (N_x - 2), (N_w + N_o))$ (Region V in Figure 6): The term

$\triangle \dot{m}_{conv}^{(k,l)}$ is identical to that in Eq. 30. The term

$$\triangle \dot{m}_{non-conv}^{(k,l)} = -\bar{\rho}^{(k,l)} v_a^{(k,l)} A_{top}^{(k,l-1)}, \tag{34}$$

where there is no positive contribution in $\triangle \dot{m}_{non-conv}^{(k,l)}$ because the top surfaces of the control volumes have no water droplets traveling downwards from the top.

For control volumes $((N_x - 1), 1 \ldots (N_w + N_o))$ (Region VI in Figure 6): All entries in $\triangle \dot{m}_{non-conv}^{(k,l)}$ are assumed 0 as non-convective flows are negligible close to the weir as fluids have much larger vertical convective flows in directions opposite to the non-convective flows. The term

$$\triangle \dot{m}_{conv}^{(N_x-1,l)} = \bar{\rho}^{(N_x-2,l)} q_{x,left}^{(N_x-1,l)} + \bar{\rho}^{(N_x-1,l+1)} q_{x,top}^{(N_x-1,l)} - \bar{\rho}^{(N_x-1,l)} q_{x,bottom}^{(N_x-1,l)}, \tag{35}$$

for all $l \in [1 \ldots (N_w - 1)]$, where $q_{x,top}^{(N_x-1,l)}$ and $q_{x,bottom}^{(N_x-1,l)}$ denote top and bottom flows downwards, respectively. The term $q_{x,bottom}^{(N_x-1,l)}$ for $l = 1$ is F_{water}. The term

$$\triangle \dot{m}_{conv}^{(N_x-1,N_w)} = \bar{\rho}^{(N_x-2,N_w)} q_{x,left}^{(N_x-1,N_w)} - \bar{\rho}^{(N_x-1,N_w)} q_{x,bottom}^{(N_x-1,N_w)}. \tag{36}$$

In the oil layer, $q_{x,top}^{(N_x-1,l)}$ and $q_{x,bottom}^{(N_x-1,l)}$ flows are upwards. The terms

$$\triangle \dot{m}_{conv}^{(N_x-1,N_w+1)} = \bar{\rho}^{(N_x-2,N_w+1)} q_{x,left}^{(N_x-1,N_w+1)} - \bar{\rho}^{(N_x-1,N_w+1)} q_{x,top}^{(N_x-1,N_w+1)}, \tag{37}$$

$$\triangle \dot{m}_{conv}^{(N_x-1,l)} = \bar{\rho}^{(N_x-2,l)} q_{x,left}^{(N_x-1,l)} + \bar{\rho}^{(N_x-1,l-1)} q_{x,bottom}^{(N_x-1,l)} - \bar{\rho}^{(N_x-1,l)} q_{x,top}^{(N_x-1,l)}, \tag{38}$$

for all $l \in [(N_w + 2) \ldots (N_w + N_o - 1)]$, and

$$\triangle \dot{m}_{conv}^{(N_x-1,N_w+N_o)} = \bar{\rho}^{(N_x-2,N_w+N_o)} q_{x,left}^{(N_x-1,N_w+N_o)} + \bar{\rho}^{(N_x-1,N_w+N_o-1)} q_{x,bottom}^{(N_x-1,N_w+N_o)}$$
$$- \bar{\rho}^{(N_x-1,N_w+N_o)} F_{oil}. \tag{39}$$

For control volumes $(N_x, 1 \ldots (N_w + N_o))$ (Region VII in Figure 6): All entries in $\triangle \dot{m}_{non-conv}^{(k,l)}$ are 0. For control volume $(N_x, N_w + N_o)$, the term

$$\triangle \dot{m}_{conv}^{(k,l)} = \bar{\rho}^{(k-1,l)} F_{oil} - \bar{\rho}^{(k,l)} F_{oil}, \tag{40}$$

and for control volume $(N_x, 1 \ldots (N_w + N_o - 1))$, the term

$$\triangle \dot{m}_{conv}^{(k,l)} = \bar{\rho}^{(k,l+1)} F_{oil} - \bar{\rho}^{(k,l)} F_{oil}. \tag{41}$$

Oil level

For the oil level equation, we write a mass balance for the total liquids in the separator. Since we consider the liquids incompressible i.e. liquid volume is conserved, a mass balance equation can be replaced by an equation for rate of change of liquid volume V_l as

$$\frac{dV_l}{dt} = F_{in}^l - F_{water} - F_{oil}. \tag{42}$$

Using trigonometric relations for the cylindrical geometry of the separator, a relationship between the liquid volume and the oil level can be established as

$$\frac{dh_{oil}}{dt} = \frac{1}{2L\sqrt{h_{oil}(2r - h_{oil})}} \frac{dV_l}{dt} = \frac{F_{in}^l - F_{water} - F_{oil}}{2L\sqrt{h_{oil}(2r - h_{oil})}}, \tag{43}$$

where r denotes the radius of the separator and L the length of the separator.

Water level

An approach similar to that for the oil level equation can be applied to obtain the water level equation. The rate of change of water layer volume V_w is expressed as

$$\frac{dV_w}{dt} = F_{in}^{wl} - F_{water} + \left(q_{w,int,\downarrow}^{(k,l)} - q_{o,int,\uparrow}^{(k,l)} \right), \tag{44}$$

which can be reformulated as

$$\frac{dh_{water}}{dt} = \frac{F_{in}^{wl} - F_{water} + q_{w,int,\downarrow}^{(k,l)} - q_{o,int,\uparrow}^{(k,l)}}{2L\left(\frac{N_x-1}{N_x}\right)\sqrt{h_{water}\left(2r - h_{water}\right)}} \tag{45}$$

assuming a perfectly cylindrical tank. Since the separator length for water level calculation is on the left of the weir, the length L has been shortened by one control volume length using the factor $\left(\frac{N_x-1}{N_x}\right)$.

Pressure

We assume that the gas phase flashes out completely at the inlet part of the separator and no reactions take place. A mass balance on the gas then becomes equivalent to a balance on moles of gas n_g inside the separator

$$\frac{dn_g}{dt} = \dot{n}_g^{in} - \dot{n}_g^{out}. \tag{46}$$

Employing the ideal gas law, we obtain

$$\frac{d}{dt}\left(\frac{P_gV_g}{R_gT}\right) = \left(\frac{P_{in}F_{in}^g}{R_gT}\right) - \left(\frac{P_gF_{out}^g}{R_gT}\right), \tag{47}$$

where R_g denotes the universal gas constant and T temperature. Since R_g and T are assumed to be constant, this simplifies to

$$\frac{d\left(P_gV_g\right)}{dt} = \left(P_{in}F_{in}^g - P_gF_{out}^g\right). \tag{48}$$

By applying chain rule to the left hand side, we get

$$V_g\frac{dP_g}{dt} + P_g\frac{dV_g}{dt} = \left(P_{in}F_{in}^g - P_gF_{out}^g\right), \tag{49}$$

Since the total separator volume, $V_{sep} = V_l + V_g$, is constant, we have $\frac{dV_g}{dt} = -\frac{dV_l}{dt}$. Inserting this relationship, we obtain

$$\frac{dP_g}{dt} = \frac{1}{V_g}\left(P_{in}F_{in}^g - P_g F_{out}^g + P_g\frac{dV_l}{dt}\right),\tag{50}$$

which when reformulated using Eq. 42, gives

$$\frac{dP_g}{dt} = \frac{1}{V_g}\left(P_{in}F_{in}^g - P_g F_{out}^g + P_g\left(F_{in}^l - F_{water} - F_{oil}\right)\right).\tag{51}$$

Optimal operation of a subsea separation system

Separation system overview

In this work, we consider a subsea separation system as shown in Figure 7. The well stream
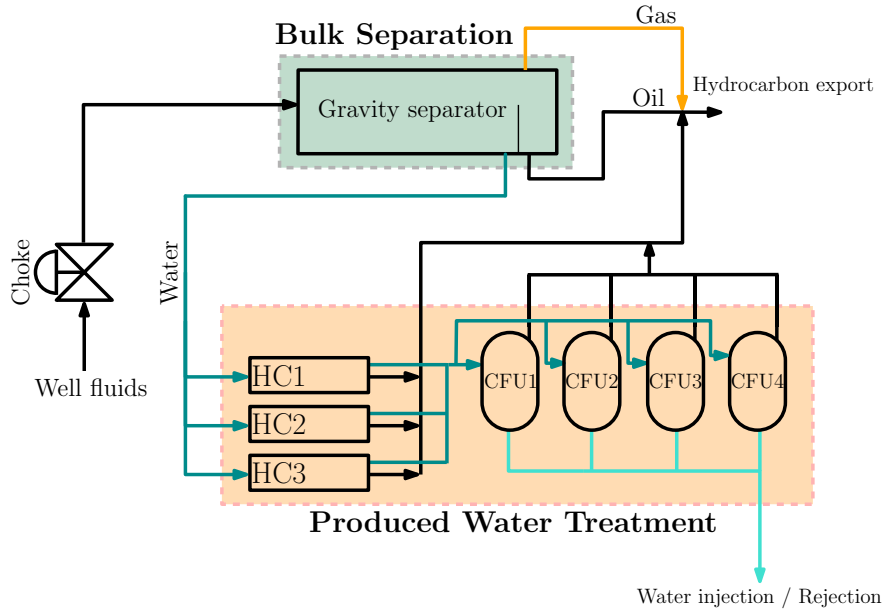

Figure 7: Our simulated subsea separation system.

containing water, oil and gas is fed to a gravity separator, in which a bulk separation into gas, oil and water phases takes place. The oil and gas streams are combined and directed to a hydrocarbon export line, while the water stream is further cleaned in three hydrocyclones

in parallel, before being purified to the final specifications in four compact flotation units. The purified water is then injected to the reservoir, or discarded into the sea. Below we describe the different parts of the separation system in more detail.

Bulk separation

In the bulk separation, a multiphase mixture of oil, water and gas undergoes a preliminary separation into gas, oil and water in a gravity separator. Since this separation is fairly crude, the concentrations of oil dispersed in water and of water dispersed in oil are relatively high. The water separated in the gravity separator is cleaned further in produced water treatment section. The separated gas, the separated oil and rejects from the produced water treatment are directed into the transport line.

Produced water treatment

In western Europe, discharging produced water containing oil concentrations above 30 ppm into the sea is not permitted.[29] Hence, in our produced water treatment, the water produced from the bulk separation goes through additional cleaning in hydrocyclones and compact flotation units. The hydrocyclones reduce the oil concentration in water to below 100 ppm. Next, the water is further purified in a compact flotation unit, which decreases the oil content below the discharge limit of 30 ppm.

Hydrocyclone: Inline deoiling hydrocyclones use a swirl element at the inlet of the hydrocyclone to put the flow into a swirling motion. Because of the angular velocity of the bulk fluid, the dispersed oil droplets are radially accelerated towards the center. The oil phase accumulates near the axial center and is removed in a separate flow (overflow, f_{over}). The rest of the flow continues into an underflow, f_{under}, as shown in Figure 8. The underflow is the purified water with an oil concentration below 100 ppm. The overflow is directed into the export line for transport to the topside or shore.

In the literature for HC modeling, data driven models are more prevalent in comparison to
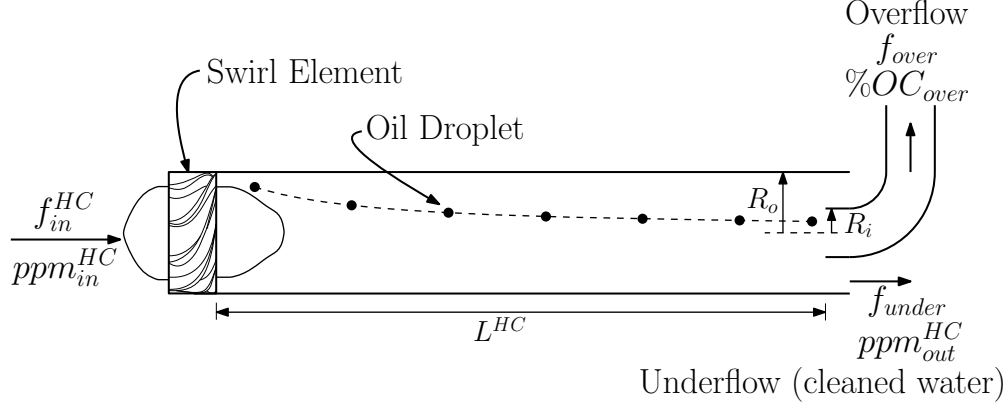
Figure 8: Schematic of an inline deoiling hydrocyclone, where L^{HC}, R_o, and R_i represent dimensions. f_{over} denotes overflow, f_{under} underflow, f_{in}^{HC} water feed flow, ppm_{in}^{HC} oil concentration in water feed, ppm_{out}^{HC} oil concentration in underflow and $\%OC_{over}$ percentage of oil fraction in overflow.

first principles models.[30] However, they are known to be valid in a short range of operating conditions.[31] Hence, in this paper, we use a simplified first-principles based hydrocyclone model developed by Das and Jäschke.[32]

Compact flotation unit: The required level of 30 *ppm* oil concentration in water can potentially be attained with HCs. However, it is customary to use another step of water treatment, such as a CFU, to have added flexibility in the system to handle disturbances and to ensure an oil concentration below 30 *ppm* under all circumstances. A schematic of a CFU is shown in Figure 9. In a CFU, a water feed with dispersed oil droplets first undergoes a swirl motion, which leads to a fraction of oil getting separated and traveling upwards. The rest of the water with an oil concentration lower than that in the feed flows downwards and is contacted with a counter-flowing gas dispersed from the bottom. The gas forms small bubbles (free bubbles), attach to the downward flowing oil droplets to form loaded bubbles, and float them to the top. At the top of the CFU, the gas, the oil and some water is removed in a stream called reject. The purified water exits the separator from the bottom.

In this paper, we used a simplified first-principles based CFU model, developed by Das and Jäschke.[33] Other control oriented models for CFUs in the literature are data driven. Please refer to Arvoh et al.,[34] Arvoh et al.[35] and Asdahl and Rabe[36] for an overview of data
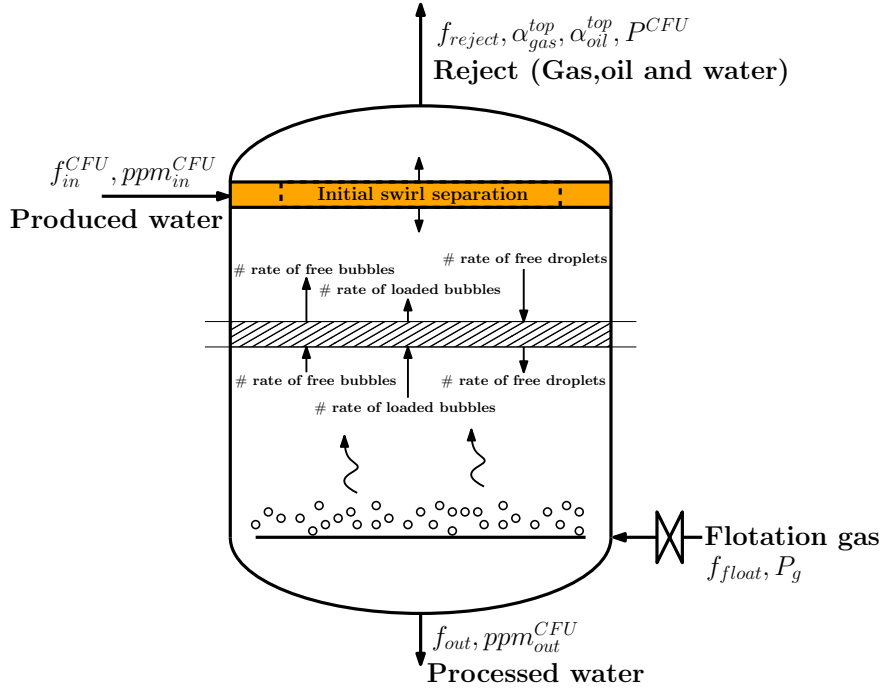
Figure 9: A schematic of a CFU. f_{in}^{CFU} denotes water inflow, ppm_{in}^{CFU} oil concentration in water feed, f_{out} processed water outflow, ppm_{out}^{CFU} oil concentration in water outflow, f_{float} flotation gas inflow at supply pressure P_g, f_{reject} reject flow at pressure P^{CFU} having a gas volume fraction of α_{gas}^{top} and an oil volume fraction of α_{oil}^{top}. The water volume fraction in the reject flow is $\alpha_{water}^{top} = (1 - \alpha_{gas}^{top} - \alpha_{oil}^{top})$. The CFU is maintained at a pressure of P^{CFU} with a volumetric liquid hold-up of α_l.

driven models for CFUs and their uses.

Case study and set-up

For the simulations, we used the model parameters presented in Table 1. The final discretized model for the gravity separator consists of $N_x(N_w + N_o) = 54$ control volumes. Further, we consider the same N_d droplet classes for oil dispersed in water as well as water dispersed in oil, resulting in $N_d N_x(N_w + N_o) = 540$ differential equations, describing the change in the partial densities of the dispersed phase in each discrete cell for each of the N_d droplet classes. In addition, the equations for h_{oil}, h_{water} and P_g lead to a total of 543 model equations for

Table 1: Model parameters for gravity separator

Parameter	Symbol	Unit	Value
Separator length	L	$[m]$	15
Separator radius	r	$[m]$	2
Weir height	h_{weir}	$[m]$	2
Mass transfer coefficient for water	k_w^{int}	$[m/s]$	0.180217
Mass transfer coefficient for oil	k_o^{int}	$[m/s]$	0.198773
Temperature	T	$[K]$	328.5
Universal gas constant	R_g	$[J/mol/K]$	8.314
Fraction of water flow that enters water layer	γ_w	$[\text{-}]$	0.602039
Fraction of oil flow that enters oil layer	γ_o	$[\text{-}]$	0.99995
Phase inversion point in terms of water cut	WC_p	$[\text{-}]$	0.7
Phase inversion point in terms of oil cut	OC_p	$[\text{-}]$	0.3
Acceleration due to gravity	g	$[m/s^2]$	9.81
Density of pure water phase	ρ_w	$[kg/m^3]$	1000
Density of pure oil phase	ρ_o	$[kg/m^3]$	831.5
Molecular weight of gas phase	M_g	$[kg/mol]$	0.01604
Viscosity of pure water phase	μ_w	$[Pas]$	5×10^{-4}
Viscosity of pure oil phase	μ_o	$[Pas]$	1×10^{-3}
Coalescence reaction rate constants	k_d	$[m^3/s]$	1×10^{-8}
Diameter of base droplet class	d_A	$[\mu m]$	150
# of droplet classes	N_d	$[\text{-}]$	10
# of droplet-droplet coalescence reactions	$N_{reaction}$	$[\text{-}]$	25
# of horizontal discretizations	N_x	$[\text{-}]$	9
# of vertical discretizations in water layer	N_w	$[\text{-}]$	3
# of vertical discretizations in oil layer	N_o	$[\text{-}]$	3

the gravity separator. Other relevant outputs of the model are water quality given by

$$ppm_{out}^{GS} = OC^{(N_x-1,1)} \times 10^6, \tag{52}$$

and oil quality given by

$$\%WiO^{GS} = WC^{(N_x,1)} \times 100. \tag{53}$$

In accordance to Figure 7, the water flow coming out of the gravity separator is evenly distributed to three hydrocyclones, such that

$$f_{in}^{HC} = \frac{F_{water}}{3}, \tag{54}$$

and

$$ppm_{in}^{HC} = ppm_{out}^{GS}. \tag{55}$$

We consider three identical HCs in our HC system, hence, $F_{in}^{HC} = 3f_{in}^{HC}$, $F_{under} = 3f_{under}$, and $F_{over} = 3f_{over}$. The total cleaned water outflow from the HCs F_{under} is then distributed evenly among the CFUs;

$$f_{in}^{CFU} = \frac{F_{under}}{4}, \tag{56}$$

and

$$ppm_{in}^{CFU} = ppm_{out}^{HC}. \tag{57}$$

We consider four identical CFUs in our CFU system, hence, $F_{in}^{CFU} = 4f_{in}^{CFU}$, $F_{out} = 4f_{out}$, $F_{reject} = 4f_{reject}$, and $F_{float} = 4f_{float}$.

Control structure design

We loosely follow the top-down plant-wide control design procedure by Skogestad[37] for designing the control structure of the separation system. The procedure can be divided into the following steps:

Overall operational objective

The main objective of our subsea separation system is to maximize the flow of cleaned water out of the system. That is, we seek to maximize the operational cost given by $J = F_{out}$, subject to relevant operational constraints. Here, clean water refers to purified water that adheres to the regulatory emission standards.[29]

Degrees of freedom and constraints in the gravity separator

The control degrees of freedom in the gravity separator are the gas outflow F_{out}^g, the oil outflow F_{oil} and the water outflow F_{water}, such that $u^{GS} = [F_{out}^g \quad F_{oil} \quad F_{water}]$. The inlet conditions, such as the feed flow rate and the feed water cut are considered disturbances to the system. The weir height h_{weir} in the gravity separator is 2 m. Therefore, the oil level must be above 2 m and water level below 2 m. To keep a safety margin of 0.2 m, we constrain the oil level h_{oil} to be higher than 2.2 m and the water level h_{water} to be lower than 1.8 m. Furthermore, the oil level should be below its maximum possible value 2.5 m as a higher oil level leads to a poor gas quality and a lower buffer volume for slug handling. We consider that the separation system is situated around 50 m under the sea level, which translates into a hydrostatic pressure due to sea water of approximately 5 bar in the vicinity of the separation system. The well fluids are assumed to enter the gravity separator at a 11.07 $bara$ pressure. In order to ensure a natural flow to topside, the pressure in the separator should not drop below a critical flow assurance pressure of 6 $bara$. Keeping a safety back-off of 2 bar from the critical flow assurance pressure and accounting for a pressure drop of approximately 3 bar from the feed pressure 11.07 $bara$, we set the operating pressure P_g to 8 $bara$.

Degrees of freedom and constraints in hydrocyclones

The total flow to the HCs and CFUs is distributed evenly to each unit, therefore the stream splits are not considered as degrees of freedom. The control degree of freedom in HCs u^{HC} is flow split $FS = F_{over}/F_{in}^{HC}$. The overflow valves in HC are typically designed to operate

at flow splits in the range of approximately 1-3%.[38] To keep a flow split back off of 0.5%, we constrain the flow split between 1.5% and 2.5%.

Degrees of freedom and constraints in compact flotation units

The control degrees of freedom in CFUs are $u^{CFU} = [F_{float} \quad F_{out} \quad F_{reject}]$. We assume that the CFUs in our separation system are designed to be operated above 1 $bara$. At a pressure of 1 $bara$, solubility of methane in water is around 15-16 ppm^1 or mg/l.[39] Since, in our system, the produced gas as well as the flotation gas is methane, maintaining the CFU at a pressure any higher than 1 $bara$ will lead to additional losses in the gas transported to the topside, as at a higher pressure water dissolves more gas. Hence, we choose a CFU pressure of 1 $bara$. Further, we constrain the ppm_{out}^{CFU} to below 10 ppm. Thereby, we keep a 20 ppm back-off from the 30 ppm limit, to account for fluctuations in ppm_{out}^{CFU} due to disturbances and imperfect control. A sensor for measuring gas fraction in the reject stream is assumed to be available that can accurately sense gas fraction in a range of 25-75%. For a method on gas fraction estimation in reject stream from CFU, refer to Arvoh et al.[34] We keep a 20% back-off from both upper and lower limits so as to provide a larger window of accurate gas fraction measurement around the gas fraction set-point under transient conditions. Hence, we constrain the α_{gas}^{top} between 45% and 55%.

---

[1]The ppm contribution of the dissolved gases, such as methane is not counted in the 30 ppm limit of oil in water.[29]

Optimal steady state operation

Combining the objective function and the constraints mentioned above results in the following steady state optimization problem:

$$\max_{[u^{GS}, u^{HC}, u^{CFU}]} F_{out}$$

$$s.t. \quad \text{model equations}$$

$$2.2\ m \leq h_{oil} \leq 2.5\ m$$

$$0 \leq h_{water} \leq 1.8\ m$$

$$P_g = 8\ bara$$

$$1.5\% \leq FS \leq 2.5\%$$

$$P^{CFU} = 1\ bara$$

$$0 \leq ppm_{out}^{CFU} \leq 10$$

$$0.45 \leq \alpha_{gas}^{top} \leq 0.55$$

$$0 \leq \alpha_{oil}^{top} \leq 1$$

$$0 \leq \alpha_{water}^{top} \leq 1$$

$$(58)$$

We consider three different cases of inlet operating conditions. They are presented in Table 2. Case 1 is the nominal case, which is similar to the 1988 production data from

Table 2: Cases of inlet operating conditions

Variable	Case 1 (nominal case)	Case 2	Case 3
Liquid inflow F_{in}^{l}, $[m^3/h]$	2124.0	2336.4	2336.4
Water cut in inflow ϵ_{in}, $[\%]$	15.0	15.0	16.5

Gullfaks-A field, used by Backi et al..[14] In Case 2, the total liquid production increases over that in Case 1 by 10%, which typically happens when a new well is tied-in to an existing producing well and the entire production is routed through the existing separation system.

In Case 3, the total production is the same as that in Case 2, whereas the water cut is raised by 10% from 15% to 16.5%. This indicates that the oil production drops and the water production rises, which is a typical scenario after some years of production from an oil and gas producing field.

For each case, we solved the steady state optimization problem described in Eq. 58. The values for important process variables for Case 1 are presented in Figure 10.
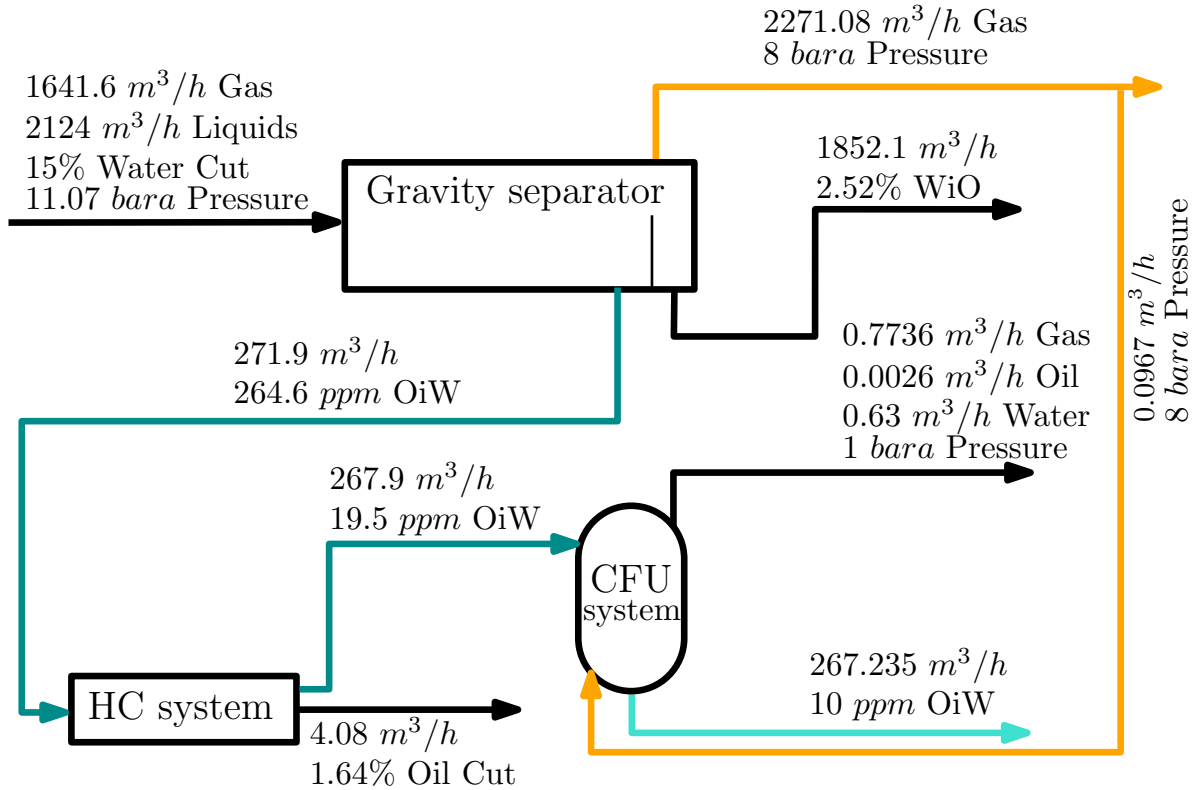

Figure 10: Optimal steady state solution for Case 1. HC system contains 3 HCs and CFU system contains 4 CFUs.

The optimal solutions for all the three cases are listed in Table 3, where separation efficiency for a separator is given by

$$\text{Separation efficiency} = \left(1 - \frac{\text{Purity of outgoing water}}{\text{Purity of incoming water}}\right). \quad (59)$$

We observe that the oil level in the gravity separator is always at its lowest value 2.2 m. As the optimization objective is to maximize the flow of cleaned water, the optimal oil level

Table 3: Optimization results for different cases

Variable	Case 1	Case 2	Case 3	Comment
Gravity separator				
h_{oil}, $[m]$	2.2	2.2	2.2	Active constraint
h_{water}, $[m]$	1.6341	1.6217	1.5854	Not active constraint
P_g, $[bara]$	8	8	8	Constrained
ppm_{out}^{GS}	264.56	272.80	251.86	
Hydrocyclone				
ppm_{out}^{HC}	19.51	22.25	25.07	
FS	1.5%	1.5%	1.5%	Active constraint
Separation efficiency	92.625%	91.846%	90.046%	
Compact flotation unit				
P^{CFU}, $[bara]$	1	1	1	Constrained
ppm_{out}^{CFU}	10	10	10	Active constraint
α_{gas}^{top}	0.55	0.55	0.55	Active constraint
Separation efficiency	48.750%	55.046%	60.113%	
F_{out}, $[m^3/h]$	267.235	289.055	319.990	Objective function
% of net water inflow cleaned	83.88%	82.48%	83.01%	

is determined by three competing effects - a higher residence time due to a higher level, a shorter vertical distance to oil-water interface due to a lower level and a higher transfer area if the level is closer to the center of the separator. In this case considered here, the second and the third reasons dominate. Similar competing effects are affecting the optimal water level, but for the operating conditions considered here, the optimal water level is not at a constraint, but is varying with changing disturbance values.

For a higher liquid inflow (Case 2) or a higher inlet water cut (Case 3), the separation load increases, which causes the oil concentration in the HC underflow, ppm_{out}^{HC}, to rise. The separation efficiency of the hydrocyclones gets worse, which is then made up by an increased separation efficiency of CFUs, due to the use of additional flotation gas.

The optimal solutions for gas hold up top in CFU for all the three cases lie at its maximum value 0.55. A higher gas hold up at the top in the CFU leads to a lower water hold up at the top, and hence a lower water loss in the reject stream. At the optimal solution, the oil content in the cleaned water from the CFU ppm_{out}^{CFU} is active at its upper limit of 10

ppm. This is due to two reasons - cleaning the water to below 10 *ppm* will require additional flotation gas, which will lead to a higher water loss in the reject stream, and discharging the highest permissible concentration of oil in the processed water will increase the total flow rate F_{out}.

Steady state concentration profiles inside gravity separator: For Case 1, the optimal steady state distributions of the droplet classes in all control volumes in the gravity separator are shown as logarithm of the number densities in Figure 11. As the feed contains
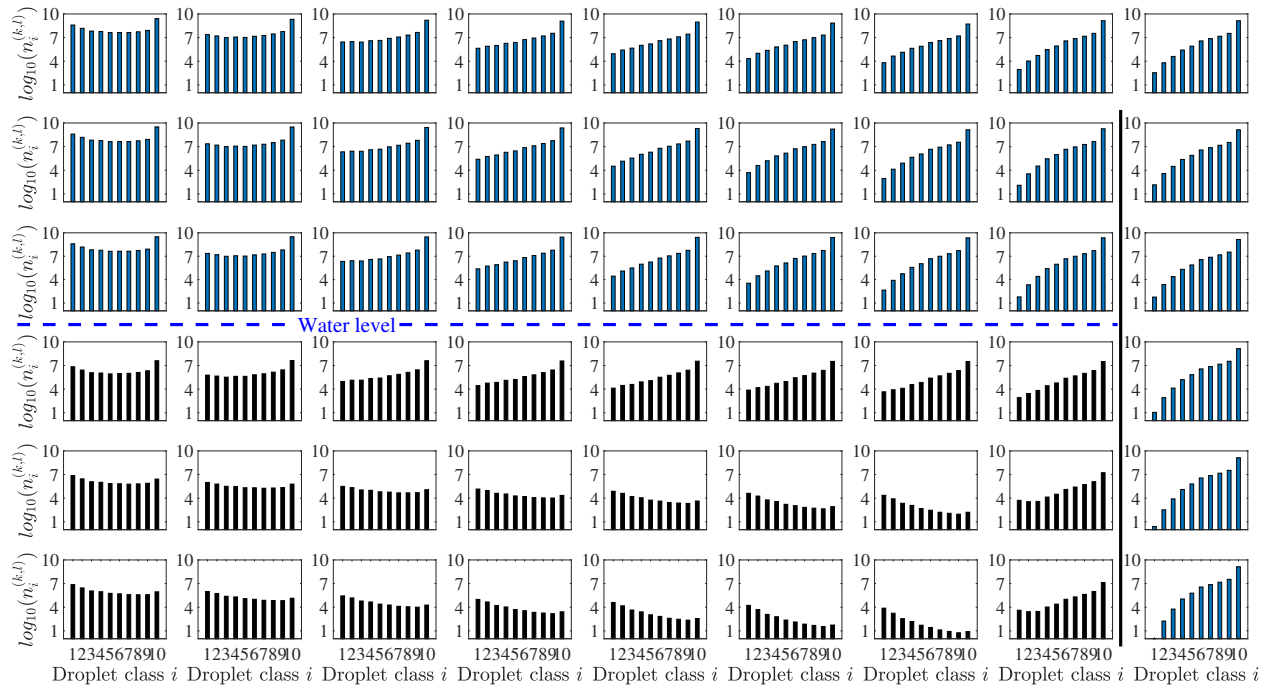

Figure 11: Dispersed phase number densities in all control volumes in the gravity separator corresponding to the optimal steady state for Case 1. The weir is indicated by a black line. The droplet sizes are [150, 189.0, 216.3, 238.5, 256.5, 272.6, 286.9, 300.0, 312.0, 323.2] μm.

only the lowest droplet class, all the leftmost control volumes have a relatively high number densities of small droplets. From left to right control volumes, we notice a reduction of small and medium sized droplets. This trend is a combined effect of the loss due to droplet-droplet coalescence and non-convective flow of droplets. In the medium to large droplet classes, the loss due to non-convective flow is somewhat compensated by the gain due to coalescence. Hence, the reduction in the number densities from left to right control volumes is not stark,

especially in the oil layer.

In the water layer, the non-convective flows are relatively large. Hence, we see a continuous drop in the number densities of the medium to large droplet classes, in particular in the bottom two layers of control volumes. On the other hand, the number densities of the largest droplet class are relatively high in the control volumes adjacent to the oil-water interface. This is due to an accumulation of droplets resulting from no loss due to coalescence and a poor mass transport across the interface. In the oil layer, the water content increases from top to bottom control volumes due to the non-convective flow and a relatively slow mass transport of water droplets across the oil-water interface to the continuous water layer.

A similar but inverted trend can be seen in the oil droplets in the continuous water in the lower half of the Figure 11. However, a trend that is slightly different for the water layer in comparison to the oil layer is relatively high number densities of the smallest droplet class well into the rightmost control volumes. This is a result of a slower coalescence, which happens because the oil fraction entering the water layer in the main separation zone is much lower than the water concentration entering the oil layer. This is because we assume that this separator is designed to produce a much cleaner water phase in comparison to the oil phase as water cleaning is the focus of our separation system. Besides, the sizes of the control volumes in water layer are larger than those in the oil layer, which makes the droplets travel longer distances vertically before they cross control volume boundaries and reach the oil-water interface. From bottom to top control volumes in water layer, the number densities for all classes increase due to an accumulation of droplets and a relatively slow mass transport of oil droplets across the oil-water interface to the continuous oil layer.

In the control volumes adjacent to the left of weir, we see an accumulation of the medium to large sized droplets, as also represented visually in Figure 4. This is because of the droplet-droplet coalescence and no non-convective flows, including no mass transfer across the oil-water interface. In all the control volumes to the right of weir, the net oil content is the same as no non-convective flows are considered in these control volumes, however,

coalescence is still active, as can be seen in the disappearance of the smallest droplet class from top to bottom.

Overall control structure and suggested pairings

The proposed control structure for the entire separation system is presented in Figure 12. The control pairings for each of the separators are explained in detail below.
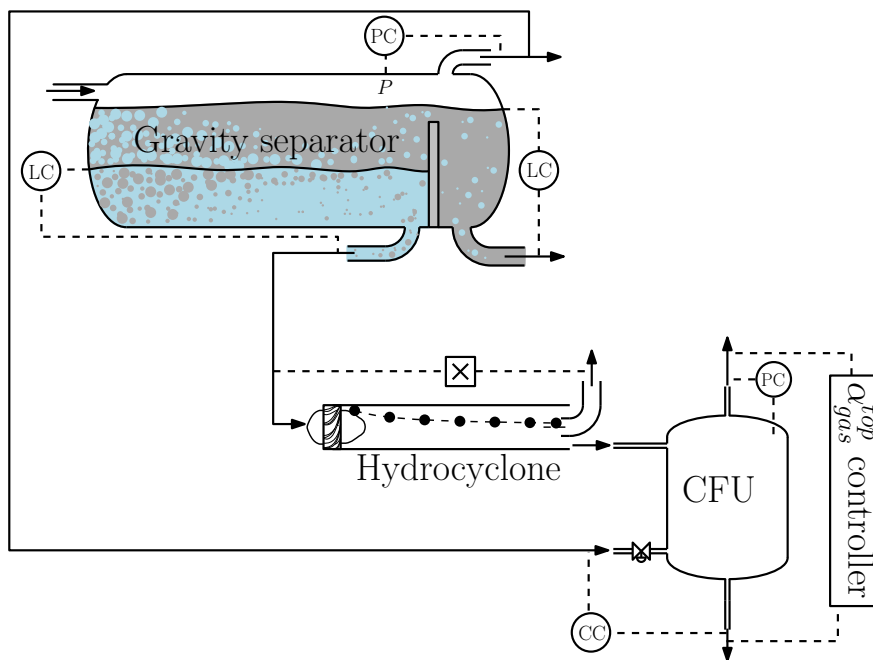
Figure 12: Control structure for the separation system with decentralized controllers for each separator. For all the regulatory controllers, it is assumed that the flow controllers are perfect, meaning there are no dynamics from the flow controllers to the actuators.

Gravity separator: The pressure P_g reflects the gas inventory and is constrained for all conditions. It is controlled using the gas outflow F_{out}^g. The water inventory reflected in h_{water} is not active constraint, and should optimally vary under operation. It is controlled using the water outflow F_{water}. However, to optimally update the level according to the current operating conditions requires solving the optimization problem whenever the conditions change. This is not desirable for practical applications. Therefore, we propose to keep it at the nominally optimal set-point. This will result in suboptimal performance. We will later show that the resulting loss is very small. The overall liquid level h_{oil} is also an active

constraint, and is controlled by the oil outflow F_{oil}. The resulting pairings are

$$P_g \to F_{out}^g, \tag{60}$$

$$h_{oil} \to F_{oil}, \tag{61}$$

and

$$h_{water} \to F_{water}. \tag{62}$$

Hydrocyclones: We suggest a flow split controller with a set point of 1.5% as found in the optimization results. This controller adjusts the overflow F_{over}. In practice, a pressure drop ratio (PDR) controller with a constant PDR set point is typically implemented[3–5] for the same and is shown to be equivalent to a flow split controller.[38] Since pressures are not modeled in the hydrocyclone model we use, we simulate the hydrocyclones using flow split controllers.

Compact flotation units: Based on the optimization results, we choose to control the variables that lie active at their constraints. These variables are ppm_{out}^{CFU}, α_{gas}^{top} and P^{CFU}. We propose to pair P^{CFU} and ppm_{out}^{CFU} with F_{reject} and F_{float},[33] respectively. The remaining degree of freedom F_{out} is used to control the gas hold up at the top α_{gas}^{top}. Hence, the resulting pairings are

$$ppm_{out}^{CFU} \to F_{float}, \tag{63}$$

$$P^{CFU} \to F_{reject}, \tag{64}$$

and

$$\alpha_{gas}^{top} \to F_{out}. \tag{65}$$

Analysis of the proposed control structure

Adjusting the set points to their optimal values whenever the disturbances change is not desirable in a real world application. Solving the nonlinear optimization problem in Eq. 58 every time the operating conditions change is impractical in most real-world applications due to the increased complexity and necessary hardware. For the disturbances considered here, the active constraints do not change, and therefore, controlling them at their bounds is always optimal. As shown in Table 3, there is only one variable not active at its constraint at the solution of Eq. 58. That variable is water level in the gravity separator, which is controlled using water outflow from gravity separator F_{water}. The optimal nominal value of h_{water} is shown in Table 3. By keeping h_{water} constant at its nominal set-point of 1.6341 m,

Table 4: Loss in objective function value as a result of using the proposed control structure for different combinations of disturbances

Liquid inflow F_{in}^l $\rightarrow$ Water cut in ϵ_{in} $\downarrow$	Nominal -10%	Nominal	Nominal $+10\%$	Average loss in F_{out} (m^3/h)
Nominal -10%	0.0522	0.0319	0.0186	0.0342
Nominal	0.0045	0.0000	0.0033	0.0026
Nominal $+10\%$	0.0067	0.0270	0.0556	0.0298
Average loss in F_{out} (m^3/h)	0.0211	0.0197	0.0258	0.0222

we obtained an overall average loss in CFU water outflow F_{out} of 0.0222 m^3/h compared to its optimal value, see Table 4, which shows loss as optimal objective function value minus the objective function value if the set-points for the nominal case are used. Considering that the optimal flow rate of purified water (the objective) is in the range of 218.63 to 319.99 m^3/h with an average value of 267.05 m^3/h, the average loss is 0.0083% of the average cleaned water flow rate. We consider it a very small and acceptable loss and hence, we conclude that the control structure is self-optimizing.[40–42] That is, the additional effort required to optimally update the water level set-point is not justified by the gain in separation performance.

Controller tunings

We select PI controllers of the form $K_c(1 + \frac{1}{\tau_I s})$ for all feed-back control loops shown in Figure 12, where K_c denotes proportional gain for the controller and τ_I integral time. The tunings have been found using SIMC rules by Skogestad[43] and are given in Table 5.

Table 5: Controller tunings using SIMC rules

Controlled variable	Manipulated variable	K_c	τ_I (sec)	τ_c (sec)
P_g [bara]	F_{out}^g [m^3/s]	-1935	20	5
h_{oil} [m]	F_{oil} [m^3/s]	-0.6	400	100
h_{water} [m]	F_{water} [m^3/s]	-0.0275	8000	2000
ppm_{out}^{CFU}	F_{float} [m^3/h]	-0.0665	2000	500
P^{CFU} [bara]	F_{reject} [m^3/h]	-9.2325	400	100
α_{gas}^{top}	F_{out} [m^3/h]	-15.3846	100	25

Closed loop simulation results

In Figures 13 - 16, we show how the system reacts dynamically to changes in inlet operating conditions, starting from Case 1, and going to Case 2 and then to Case 3 in steps at 4 h and 18 h, respectively. Though step disturbances are unlikely in real applications, we use them to demonstrate the behavior of the controllers. In addition, we introduce step changes in the set-points of the oil level and the water level in the gravity separator at 35 h and 40.55 h, respectively in order to demonstrate the behavior of the gravity separator model. Below we consider results for each separator individually.

Gravity separator

Figure 13 shows the results for the gravity separator. At 2 h, the gas inflow is raised, which causes the pressure controller to increase the gas outflow. At the transition from Case 1 to Case 2, the throughput is raised. Subsequently, the water in oil and oil in water in the outlets increase as a higher throughput causes a reduction in residence time for the fluids in the separator, causing a poorer separation performance. The inverse responses in the oil in water and water in oil on introduction of Case 2 are due to the fact that the disturbances in
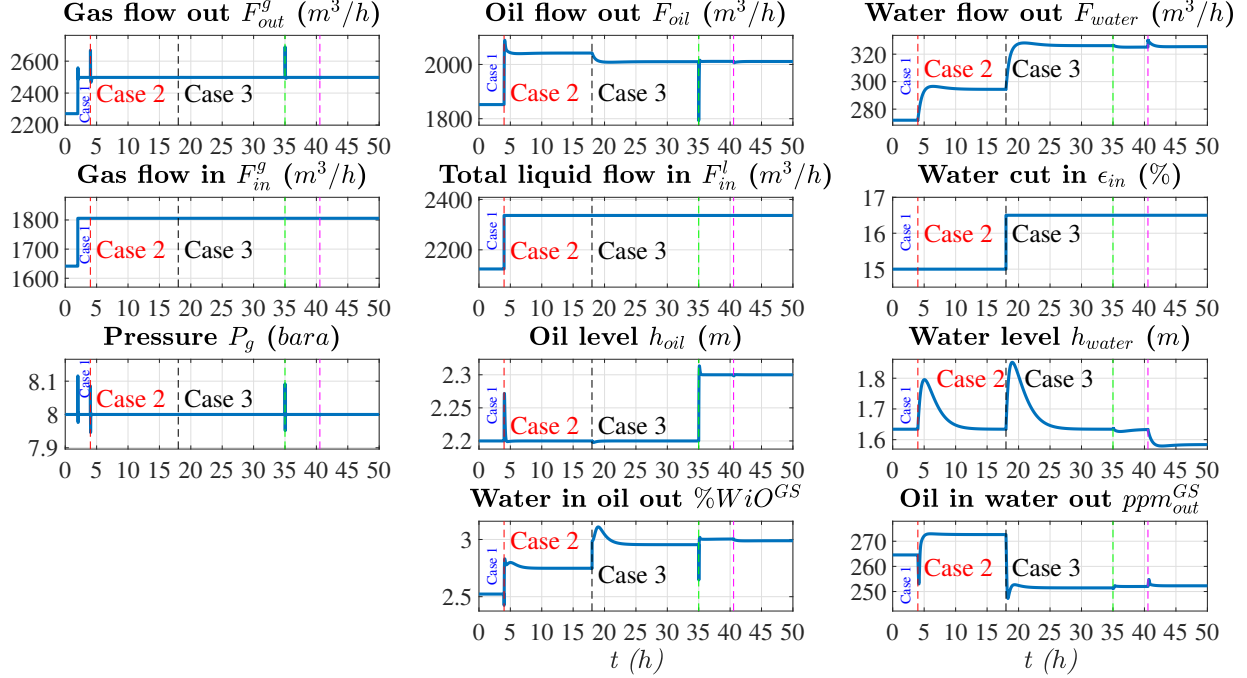
Figure 13: Closed loop results for gravity separator.

the inlet conditions cause the levels to rise beyond their set-points transiently, which makes the control volumes to increase in size everywhere in the separator whereas the dispersed fluids at the inlet take some time to reach the outlet. With the same dispersed phase masses in the control volumes close to the outlet and increased transient control volume sizes, the concentration first drops before reaching a new higher steady state later. The slow control of oil level causes the oil flow to react somewhat slowly, whereas the response in the water level is even slower due to an even slower control loop.

In Case 3, the inflow of water into the separator increases and that of oil reduces, which can be seen in the respective outflows as well. This leads to a reduced residence time of fluids in the water layer and a reduced concentration of oil into the water layer at the inlet. Overall, we see that the latter is the dominant effect as the oil concentration in the water outlet decreases. On the other hand, in the oil layer, the residence time of fluids is reduced and the concentration of water entering the oil layer at the inlet increases, leading to an increased water concentration in the oil outlet.

The increase in oil level set-point at 35 h causes the separation to get worse. The water

content in the oil outflow increases due to fewer water droplets getting separated, having to travel a longer distance to reach the interface. The oil content in the water outflow increases due to reduced water transport into the water layer across the interface. The oil outflow increases due to additional water content in it, whereas the water outflow reduces. The water level set-point is reduced at $40.55\ h$, which causes the water in oil outlet to drop due to an increased residence time in the oil layer. The oil in water outlet rises as a reduced residence time in the water layer dominates over the increased water transport across the interface.

Concentrations profiles in selected control volumes: Figure 14 presents the results for the concentrations of oil in the water phase and water in the oil phase in selected control volumes in the gravity separator. For the control volumes from top to bottom in the oil
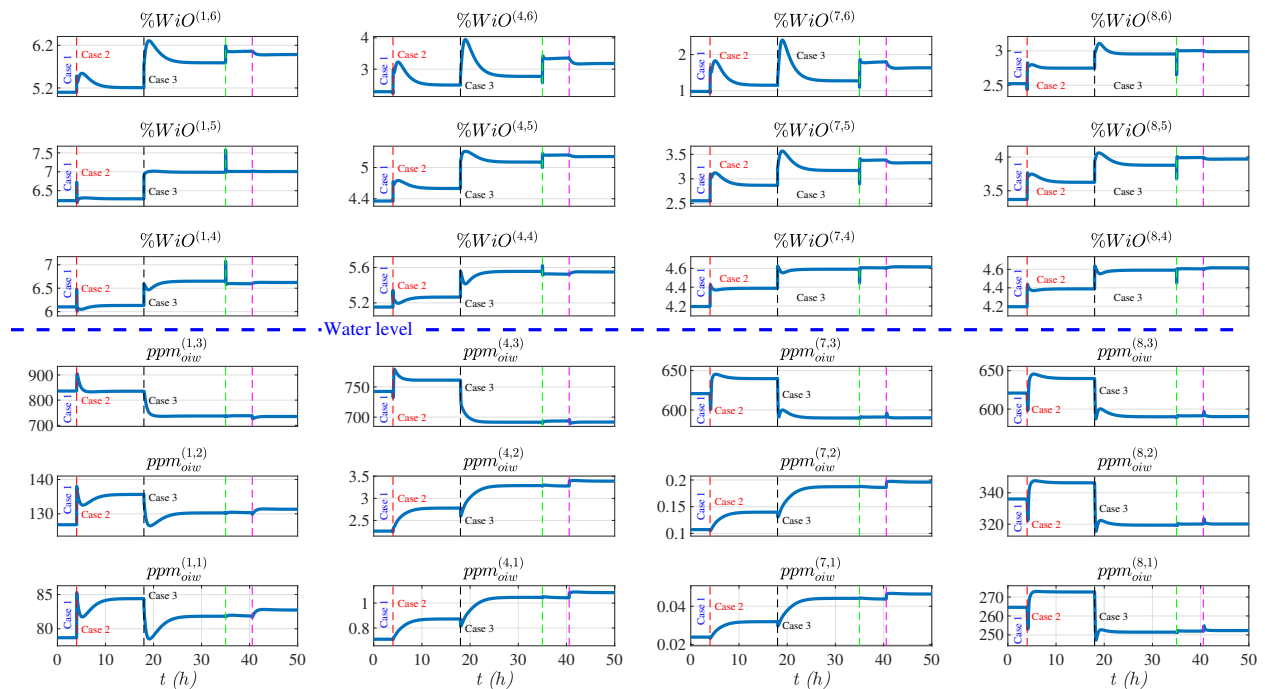

Figure 14: Dynamic responses in oil concentration in water and water concentration in oil in selected control volumes (k, l) left of the weir in the gravity separator. The water level is indicated by a blue dashed line dividing the figure in two halves, where the top half represents the oil layer and the bottom the water layer.

layer and bottom to top in the water layer, we notice an increase in the dispersed phase concentration. This is a result of an accumulation of dispersed phase due to a poor mass transport of dispersed phase into its respective continuous phase - a trend that is in agreement

with Figure 11, especially for the medium to large sized droplet classes. When the inlet operating conditions change from Case 1 to Case 2, the total liquid inflow increases. This causes the concentrations of water in oil and oil in water to increase in most of the leftmost control volumes due to a reduced residence time for separation. This trend continues into the control volumes to the right as well as in the outgoing liquid streams of oil and water.

In control volumes $(4, 1), (4, 2), (7, 1)$ and $(7, 2)$, we notice exceptionally pure water. This is an artifact of the assumptions made. In particular, it is a result of a fast coalescence of droplets and no droplet breakage. However, the outlet purities of the separator exhibit a reasonable behavior, and for the purpose of designing a control structure, this is the most important property. In future work we will modify the model to reflect the concentrations in the interior more accurately.

On the introduction of Case 3, the water cut increases i.e. the net water inflow rises and net oil inflow decreases, which causes more water to be dispersed in the oil phase and less oil to be dispersed in the water phase at the inlet of the separator. Hence, we observe a further increase in the water content in all the control volumes above the water level. Below the water level, we observe a reduction in oil concentration in all of the leftmost control volumes. However, the effect of an increased residence time is prominent in the increased oil concentration in the control volumes to the right, especially close to the bottom. Overall, the effect of the reduced oil feed to the water layer dominates, and consequently, we see a drop in the oil concentration in the water outlet.

The oil level increase at $35 \ h$ yields an increased concentration of water in oil phase due to a larger distance that water droplets need to travel to reach the oil-water interface to get separated. However, closer to the interface, we notice a small reduction of water concentration especially in the control volumes in the left. This is due to a reduced number of water droplets coming from the top having to travel a longer distance and a higher residence time for separation of water droplets in the oil phase due to a slightly reduced oil flow. But, towards the right, the accumulation takes over and we see an increased water concentration.

As a higher water concentration in the oil phase leads to a reduced water transport through the oil-water interface down to the water layer, the oil concentration increases slightly.

The water level reduction at $40.55\ h$ causes a reduction in the residence time in the water layer, which causes the oil concentration in all control volumes in water layer, except the ones at the oil-water interface, to rise due to poorer separation. Due to a higher residence time in the oil layer, more water is transported to the water layer, resulting in a reduced oil concentration in the control volumes in the water layer close to the interface. However, overall, we notice an increase in oil concentration in the water outlet, thereby confirming the dominance of the effect of the reduced residence time over other effects. As a result of an increased residence in the oil layer, the water concentrations in most of the control volumes are reduced. However, in the control volumes next to the interface, the water concentration rises marginally as an accumulation of the water droplets arriving from the top edges dominates over the increased water transport across the interface.

Hydrocyclone

Figure 15 shows the results for the HC. The introduction of Case 2 causes an increase in feed flow as well as in feed oil concentration in water, which implies a higher load on the HC. The overflow F_{over} is adjusted such that it is equal to the product of inflow F_{in}^{HC} and a given set-point (1.5%) for the flow split F_{over}/F_{in}^{HC}. The oil in water at the outlet rises due to a poorer separation efficiency. The introduction of Case 3 causes an increase in feed flow and a reduction in feed oil concentration in water. The increased feed flow causes the overflow to increase. The resulting response of a higher oil content in the underflow despite a reduced oil concentration in the inflow is a result of a poorer separation due to a higher throughput.

The increase of oil level set-point in the gravity separator causes a reduction in the water flow, with an increase in the oil concentration therein, fed to the HC. This improves the separation efficiency of the HC and we see a reduced oil concentration in the underflow. The
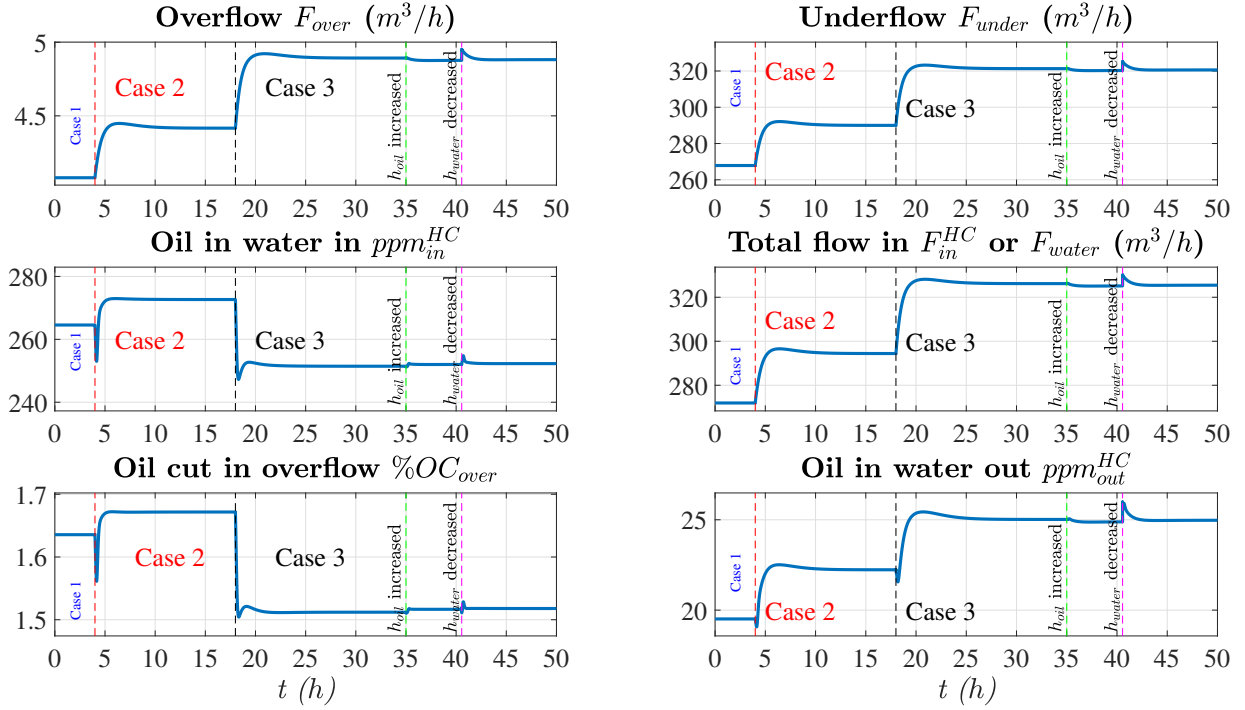
Figure 15: Closed loop results for hydrocyclones.

reduction in water level set-point in the gravity separator causes both the flow and the oil concentration of the water feed to the HC to increase. This affects the separation efficiency of the HC adversely and the oil content in the underflow rises.

Compact flotation unit

Figure 16 shows the results for CFU. The underflow water from the outlet of hydrocyclones enter the CFUs. The pressure and the gas hold up top are controlled at constant set-points using reject flow and water outflow, respectively. The set-point for the gas hold up at the top is kept at its upper bound of 55%. The flotation gas flow is used as a manipulated variable to control the oil content in the water at the outlet. This loop is tuned slower than the other loops because a change in flotation gas inflow acts as a huge disturbance for the other two loops, which are expected to react quickly to satisfy the operational constraints on the pressure and the gas hold up at top. In other words, tight control of the pressure and the gas hold up top under transient conditions is prioritized over tight control of ppm_{out}^{CFU}.
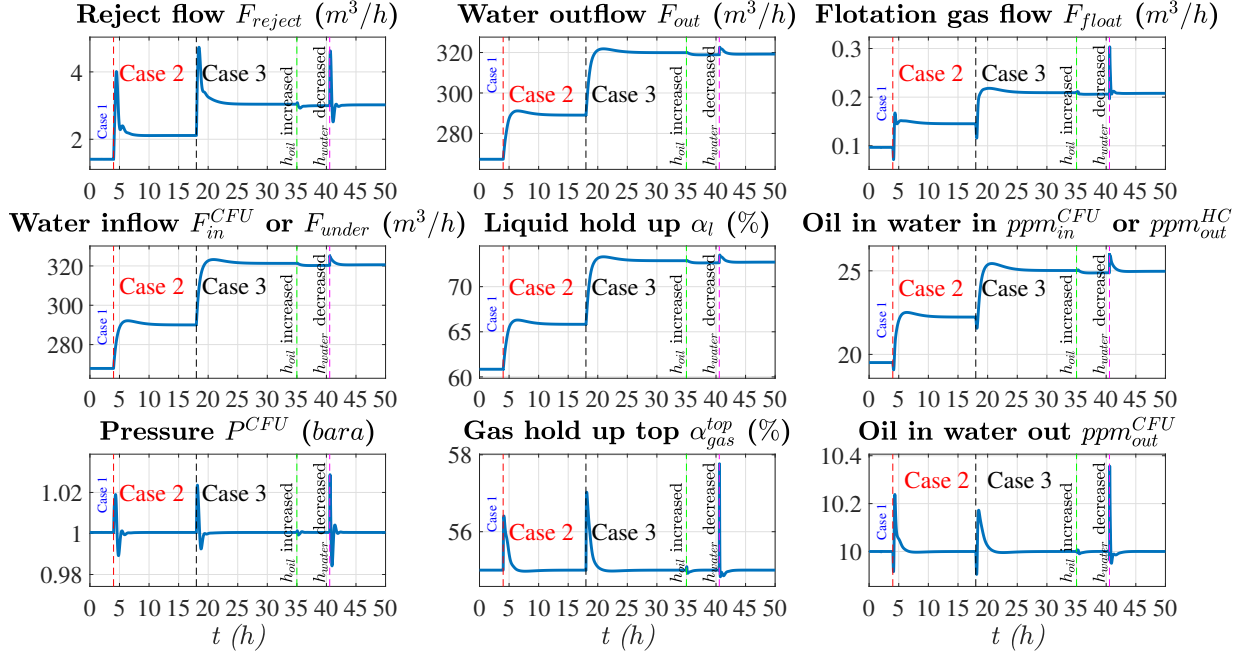
Figure 16: Closed loop results for compact flotation unit with regulatory control of pressure, gas hold-up top and ppm_{out}^{CFU}.

On transition from Case 1 to Case 2, the water inflow and the incoming oil in water increases, causing a larger load on the CFU. Hence, the need for flotation gas flow increases. The reject stream is a vent for the gas inventory, hence the reject flow increases too in order to keep the pressure constant. Due to an increased gas inflow, the gas hold up at the top rapidly increases before it is brought back to its set point of 55% with an increased water outflow. A similar trend is observed at the introduction of Case 3 because the nature of the incoming disturbances are similar.

The increase of the oil level set-point in the gravity separator causes a reduced separation load on the CFU, which results in a reduced flotation gas usage and hence, a reduced reject flow. The reduction of the water level set-point in the gravity separator increases the separation load on the CFU, which increases the flotation gas usage and the reject flow. Since the water level controller in the gravity separator is tuned much slower than the oil level controller, the disturbances arriving to the CFU due to water level changes are much slower. Hence, it takes longer to reject those disturbances in the CFU.

In terms of optimal operation, we noticed that the values of the objective function, the water outflow from CFU for the different cases - 289.05 m^3/h for Case 2 and 319.94 m^3/h for Case 3 - are very close to the optimal values reported in Table 3. This is in agreement with the analysis of the control structure presented earlier.

Discussion

Necessarily, the model developed for the gravity separator has many simplifying assumptions. The influence of thermodynamics is ignored in the model, which if considered will affect the chemical compositions in the continuous as well as dispersed parts of the two phases - oil and water as a function of pressure and temperature in the separator. The gas phase will have a composition determined by fractions of components that are not dissolved in either water or oil. Since the pressure in the separator is tightly controlled, it can be assumed constant and the temperature is given by that of the incoming flow, which also does not change rapidly. Hence, for most practical purposes, the compositions of the three phases at the inlet of the separator can be considered constant if there are no fluctuations in the composition of the incoming well fluids. The inlet compositions will then decide the physical properties, such as viscosities and densities of the phases. If the physical properties as determined by thermodynamics are included, the rest of the model will be valid in its current state.

The model also assumes a fixed base droplet size and a finite set of droplet classes, which will not be true in a realistic setting. The droplet classes will be different and not discrete. Further, in this model we used a single constant value for the droplet-droplet coalescence reaction rate constant k_d. This rate constant is inversely proportional to the coalescence time t_{coal} as $k_d \propto 1/t_{coal}$, which means the lower the coalescence time, the higher the coalescence rate. Many models from literature assume that the coalescence time is proportional to the droplet size,[16,44,45] indicating that in real systems, the k_d will decrease as the droplets grow in size. However, the k_d values for all droplet classes can, in general, be raised using external

modules, such as electro-coalescers equipped in separators, or adding chemicals, such as de-emulsifiers. Lastly, the k_d values will be different for dispersed water in continuous oil and dispersed oil in continuous water and they need to be determined through experimental investigations, which is beyond the scope of this work.

In this paper, we focused on developing a model that describes coalescence phenomena in the main separation zone. The model parameters will need to be adapted to experimental data as a next step in this research. Here also model adjustments may be done to include droplet breakage terms, such that the concentration profiles in the separator are more realistic.

In the dynamic simulation results, we noticed inverse responses in the concentration variables in the gravity separators. This response may have been avoided if the levels in the separator were considered to have a wave that travels through the separator in the axial direction. However, considering the wave would have made the model much more complex, hence, a flat level was assumed, as is commonly done in literature.[11,13]

We presented results for different cases of inlet operating conditions. Our analysis suggests that the set-points of the controlled variables in the separation system do not need to be changed in order to maintain near optimal operation under changes in inlet conditions. Hence, we chose to not update the set-points when disturbances arrive. The constant set point policy (self-optimizing control) results in a very small loss, which is supported by the analysis of the control structure as well as dynamic simulations for Cases 1-3. Therefore, the control structure proposed in this paper is able to maintain near optimal operation under changing inlet operating conditions without having to change the set-points of the important controlled variables.

Conclusion

In this work, we developed a coalescence based gravity separator model, which can dynamically predict oil content in water and water content in oil to changes in inlet operating conditions and set-points for controlled variables. The model considers changes in gas inflow, total liquid inflow and water cut in the liquid inflow as disturbances, and separator pressure, oil level and water level as controlled variables.

Further, the gravity separator model has been used with existing literature models for hydrocyclones and compact flotation units, to model a subsea separation system that separates and then purifies water produced in the hydrocarbon production. This separation system has been used to optimize the process and find a control structure that enables near optimal operation, where the objective is to maximize water removal through the separation system under varying inlet operating conditions.

In the optimization results, a detailed analysis of the evolution of dispersed droplet distribution inside the gravity separator has been presented. The optimal solution for the nominal case also provided the set-points for the variables that are controlled by the regulatory control layer. Thereafter, the closed loop results for each separator are presented and discussed in detail, along with an extended analysis of the dispersed phase concentration profiles within selected control volumes inside the gravity separator. The proposed control strategy has been shown to yield near-optimal operation without the need for a supervisory RTO layer or changes to the set-points.

Acknowledgement

References

(1) Brondel, D.; Edwards, R.; Hayman, A.; Hill, D.; Mehta, S.; Semerad, T. Corrosion in the oil industry. *Oilfield review* **1994**, *6*, 4–18.

(2) Orlowski, R.; Euphemio, M. L. L.; Euphemio, M. L.; Andrade, C. A.; Guedes, F.; Tosta da Silva, L. C.; Pestana, R. G.; de Cerqueira, G.; Lourenço, I.; Pivari, A., et al. Marlim 3 phase subsea separation system-challenges and solutions for the subsea separation station to cope with process requirements. Offshore Technology Conference. 2012.

(3) Yang, Z.; Stigkær, J. P.; Løhndorf, B. Plant-wide control for better de-oiling of produced water in offshore oil & gas production. ICONS. 2013; pp 45–50.

(4) Yang, Z.; Pedersen, S.; Durdevic, P. Cleaning the produced water in offshore oil production by using plant-wide optimal control strategy. Oceans-St. John's, 2014. 2014; pp 1–10.

(5) Yang, Z.; Pedersen, S.; Durdevic, P.; Mai, C.; Hansen, L.; Jepsen, K.; Aillos, A.; Andreasen, A. Plant-wide control strategy for improving produced water treatment. **2016**,

(6) Ribeiro, C.; Miyoshi, S.; Secchi, A.; Bhaya, A. Model Predictive Control with quality requirements on petroleum production platforms. *Journal of Petroleum Science and Engineering* **2016**, *137*, 10–21.

(7) Bringedal, B.; Ingebretsen, T.; Haugen, K. Subsea Separation and Reinjection of Produced Water. Offshore Technology Conference. 1999.

(8) Baggs, C.; Kent, I.; Allen, J., et al. Troll Pilot control system: advanced control system for a subsea separator. Offshore Technology Conference. 2000.

(9) Neuenkirchen, J., et al. Tordis Subsea Separation Boosting and Injection (SSBI) Project: Project Presentation and Description of the Production Control System. Subsea Controls and Data Acquisition 2006: Controlling the Future Subsea. 2006.

(10) Gjerdseth, A. C.; Faanes, A.; Ramberg, R., et al. The Tordis IOR Project. Offshore technology conference. 2007.

(11) Sayda, A. F.; Taylor, J. H. Modeling and control of three-phase gravilty separators in oil production facilities. American Control Conference, 2007. ACC'07. 2007; pp 4847–4853.

(12) Das, T.; Backi, C. J.; Jäschke, J. *Computer Aided Chemical Engineering*; Elsevier, 2017; Vol. 40; pp 1489–1494.

(13) Backi, C. J.; Skogestad, S. A simple dynamic gravity separator model for separation efficiency evaluation incorporating level and pressure control. American Control Conference (ACC), 2017. 2017; pp 2823–2828.

(14) Backi, C. J.; Grimes, B. A.; Skogestad, S. A Control-and Estimation-Oriented Gravity Separator Model for Oil and Gas Applications Based upon First-Principles. *Industrial & Engineering Chemistry Research* **2018**, *57*, 7201–7217.

(15) Frising, T.; Noïk, C.; Dalmazzone, C. The liquid/liquid sedimentation process: from droplet coalescence to technologically enhanced water/oil emulsion gravity separators: a review. *Journal of dispersion science and technology* **2006**, *27*, 1035–1057.

(16) Chesters, A. Modelling of coalescence processes in fluid-liquid dispersions: a review of current understanding. *Chemical engineering research and design* **1991**, *69*, 259–270.

(17) Liao, Y.; Lucas, D. A literature review on mechanisms and models for the coalescence process of fluid particles. *Chemical Engineering Science* **2010**, *65*, 2851–2864.

(18) Hallanger, A.; Soenstaboe, F.; Knutsen, T., et al. A simulation model for three-phase gravity separators. SPE Annual Technical Conference and Exhibition. 1996.

(19) Hansen, E. W. Phenomenological Modelling and Simulation of Fluid Flow and Separation Behavior in Offshore Gravity Separators. *ASME-PUBLICATIONS-PVP* **2001**, *431*, 23–30.

(20) Jeelani, S. A. K.; Hartland, S. Prediction of steady state dispersion height from batch settling data. *AIChE journal* **1985**, *31*, 711–720.

(21) Jeelani, S.; Hartland, S. The continuous separation of liquid/liquid dispersions. *Chemical engineering science* **1993**, *48*, 239–254.

(22) Jeelani, S.; Hosig, R.; Windhab, E. J. Kinetics of low Reynolds number creaming and coalescence in droplet dispersions. *AIChE journal* **2005**, *51*, 149–161.

(23) Hartland, S.; Jeelani, S. Choice of model for predicting the dispersion height in liquid/liquid gravity settlers from batch settling data. *Chemical engineering science* **1987**, *42*, 1927–1938.

(24) Arntzen, R. Gravity separator revamping. Ph.D. thesis, Norwegian University of Science and Technology, 2001.

(25) Spiecker, P. M.; Gawrys, K. L.; Trail, C. B.; Kilpatrick, P. K. Effects of petroleum resins on asphaltene aggregation and water-in-oil emulsion formation. *Colloids and surfaces A: Physicochemical and engineering aspects* **2003**, *220*, 9–27.

(26) Kokal, S. L., et al. Crude oil emulsions: A state-of-the-art review. *SPE Production & facilities* **2005**, *20*, 5–13.

(27) Dudek, M.; Kancir, E.; Øye, G. Influence of the Crude Oil and Water Compositions on the Quality of Synthetic Produced Water. *Energy & Fuels* **2017**, *31*, 3708–3716.

(28) Heggheim, S. J. Modelling and Control of Coalescence Based Gravity Separators in a Subsea Separation System. M.Sc. thesis, Norwegian University of Science and Technology, Trondheim, Norway, 2018.

(29) OSPAR, Discharges, OSPAR Convention. 2001; `www.ospar.org/work-areas/oic/discharges`.

(30) Durdevic, P.; Pedersen, S.; Bram, M.; Hansen, D.; Hassan, A.; Yang, Z. Control oriented modeling of a de-oiling hydrocyclone. *IFAC-PapersOnLine* **2015**, *48*, 291–296.

(31) Durdevic, P.; Pedersen, S.; Yang, Z. Challenges in Modelling and Control of Offshore De-oiling Hydrocyclone Systems. Journal of Physics: Conference Series. 2017.

(32) Das, T.; Jäschke, J. Modeling and control of an inline deoiling hydrocyclone. *IFAC-PapersOnLine* **2018**, *51*, 138–143.

(33) Das, T.; Jäschke, J. Simplified First-Principles Model of a Compact Flotation Unit for Use in Optimization and Control. *Industrial & Engineering Chemistry Research* **2018**,

(34) Arvoh, B. K.; Asdahl, S.; Rabe, K.; Halstensen, M. Online estimation of reject gas flow rates in compact flotation units for produced water treatment: A feasibility study. *Chemometrics and Intelligent Laboratory Systems* **2012**, *114*, 87–98.

(35) Arvoh, B. K.; Asdahl, S.; Rabe, K.; Ergon, R.; Halstensen, M. Online estimation of reject gas and liquid flow rates in compact flotation units for produced water treatment. *Flow Measurement and Instrumentation* **2012**, *24*, 63–70.

(36) Asdahl, S.; Rabe, K. Real-time automatic operation and optimization of produced-water treatment. SPE Middle East Intelligent Energy Conference and Exhibition. 2013.

(37) Skogestad, S. Control structure design for complete chemical plants. *Computers & Chemical Engineering* **2004**, *28*, 219–234.

(38) Husveg, T.; Rambeau, O.; Drengstig, T.; Bilstad, T. Performance of a deoiling hydrocyclone during variable flow rates. *Minerals Engineering* **2007**, *20*, 368–379.

(39) Duan, Z.; Mao, S. A thermodynamic model for calculating methane solubility, density and gas phase composition of methane-bearing aqueous fluids from 273 to 523 K and from 1 to 2000 bar. *Geochimica et Cosmochimica Acta* **2006**, *70*, 3369–3386.

(40) Skogestad, S. Self-optimizing control: The missing link between steady-state optimization and control. *Computers & Chemical Engineering* **2000**, *24*, 569–575.

(41) Skogestad, S. Plantwide control: The search for the self-optimizing control structure. *Journal of process control* **2000**, *10*, 487–507.

(42) Jäschke, J.; Cao, Y.; Kariwala, V. Self-optimizing control–A survey. *Annual Reviews in Control* **2017**, *43*, 199–223.

(43) Skogestad, S. Simple analytic rules for model reduction and PID controller tuning. *Journal of process control* **2003**, *13*, 291–309.

(44) Hahn, P.-S.; Slattery, J. Effects of surface viscosities on the stability of a draining plane parallel liquid film as a small bubble approaches a liquid-gas interface. *AIChE journal* **1985**, *31*, 950–956.

(45) Lobo, L.; Ivanov, I.; Wasan, D. Dispersion coalescence: Kinetic stability of creamed dispersions. *AIChE journal* **1993**, *39*, 322–334.

Graphical TOC Entry